Title

Orai mediated Calcium entry sets the excitability threshold of central dopaminergic neurons by regulation of gene expression

Authors

Rishav Mitra[1], Shlesha Richhariya[1,2], Gaiti Hasan[1]

[1] National Centre for Biological Sciences, Tata Institute of Fundamental Research, Bangalore, India
[2] Department of Biology, Brandeis University, Waltham, USA

Correspondence: gaiti@ncbs.res.in

Keywords

Neuromodulation, Drosophila flight, PPL1 DANs, histone modifications, Trithorax-like

Highlights

1. Store-operated Ca^{2+} entry (SOCE) through Orai is required in a set of flight-promoting central dopaminergic neurons (fpDANs) during late pupae and early adults to establish their gene expression profile.

2. SOCE activates a homeobox transcription factor, '*Trithorax-like*' and thus regulates expression of histone modifiers Set2 and *E(z)* to generate a balance between opposing epigenetic signatures of H3K36me3 and H3K27me3 on downstream genes.

3. SOCE drives a transcriptional feedback loop to ensure expression of key genes required for neuronal function including the muscarinic acetylcholine receptor (*mAChR*) and the inositol 1,4,5-trisphosphate receptor (*itpr).*

4. The transcriptional program downstream of SOCE is key to functional maturation of the dopaminergic neurons, enabling their neuronal excitability and synaptic transmission required for adult flight.

Graphical Abstract

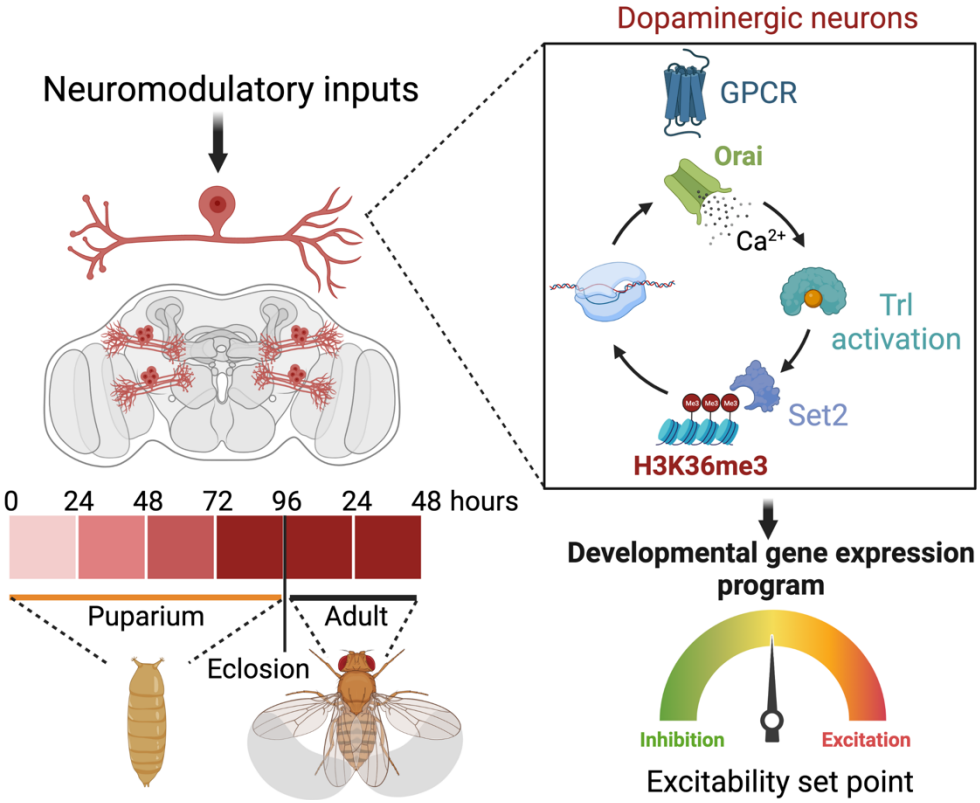

Abstract

Maturation and fine-tuning of neural circuits frequently requires neuromodulatory signals that set the excitability threshold, neuronal connectivity and synaptic strength. Here we present a mechanistic study of how neuromodulator stimulated intracellular Ca^{2+} signals, through the store - operated Ca^{2+} channel Orai, regulate intrinsic neuronal properties by control of developmental gene expression in flight promoting central dopaminergic neurons (fpDANs). The fpDANs receive cholinergic inputs for release of dopamine at a central brain tripartite synapse that sustains flight (Sharma and Hasan, 2020). Cholinergic inputs act on the muscarinic acetylcholine receptor to stimulate intracellular Ca^{2+} release through the endoplasmic reticulum (ER) localised inositol 1,4,5-trisphosphate receptor followed by ER-store depletion and Orai mediated store-operated Ca^{2+} entry (SOCE). Analysis of gene expression in fpDANs followed by genetic, cellular and molecular studies identified Orai-mediated Ca^{2+} entry as a key regulator of excitability in fpDANs during circuit maturation. SOCE activates the transcription factor Trithorax-like (Trl) which in turn drives expression of a set of genes including *Set2*, that encodes a histone 3 Lysine 36 methyltransferase (H3K36me3). Set2 function establishes a positive feedback loop,

essential for receiving neuromodulatory cholinergic inputs and sustaining SOCE. Chromatin modifying activity of Set2 changes the epigenetic status of fpDANs and drives expression of key ion channel and signaling genes thus setting the excitability threshold that determines dopamine release for maintenance of long flight.

Introduction

Neural circuitry underlying mature adult behaviours emerges from a combination of developmental gene expression programs and experience-dependent neuronal activity. Holometabolous insects such as *Drosophila*, reconfigure their nervous system during metamorphosis to generate circuitry capable of supporting adult behaviours (Levine, 1984). During pupal development, neurons undergo maturation of their electrical properties with a gradual increase in depolarizing responses and consequent synaptic transmission (Hardie et al., 1993; Jarvilehto and Finell, 1983). Apart from voltage-gated Ca^{2+} channels and fast-acting neurotransmitters specific to ionotropic receptors, the developing nervous system also uses neuromodulators, that target metabotropic receptors, show slower response kinetics and are capable of affecting a larger subset of neurons by means of diffusion aided volumetric transmission (Taber and Hurley, 2014). Although neuromodulators alter intrinsic neuronal properties (Marder, 2012) by changes in gene expression, the molecular mechanisms through which this is achieved and maintained over developmental timescales needs further understanding.

Ca^{2+} signals generated by neuronal activity can determine neurotransmitter specification (Spitzer, 2012), synaptic plasticity (O'Hare et al., 2022; Takechi et al., 1998), patterns of neurite growth (Gu and Spitzer, 1995) and gene expression programs (Ciceri et al., 2022; Rosenberg and Spitzer, 2011) over developmental timescales (McKinney et al., 2022) where output specificity is defined by signal dynamics. Neuromodulators generate intracellular Ca^{2+} signals by stimulation of cognate G-Protein Coupled Receptors (GPCRs) linked to the inositol 1,4,5-trisphosphate (IP_3) and Ca^{2+} signalling pathway. IP_3 transduces intracellular Ca^{2+} release through the endoplasmic reticulum (ER) localised ligand-gated ion channel, the inositol 1,4,5-trisphosphate receptor (IP_3R; Streb et al., 1984), followed by store-operated Ca^{2+} entry (SOCE) through the plasma membrane localised Orai channel (Prakriya and Lewis, 2015; Thillaiappan et al., 2019). Cellular and physiological

65 consequences of Ca^{2+} signals generated through SOCE exhibit different time-scales
66 and sub-cellular localisation from activity induced signals, suggesting that they alter
67 neuronal properties through novel mechanisms.

68 Expression studies, genetics and physiological analysis support a role for
69 IP_3/Ca^{2+} and SOCE in neuronal development and the regulation of adult neuronal
70 physiology across organisms (Hasan and Sharma, 2020; Mitra and Hasan, 2022;
71 Somasundaram et al., 2014). In *Drosophila*, neuromodulatory signals of
72 neurotransmitters and neuropeptides stimulate cognate GPCRs on specific neurons
73 to generate IP_3 followed by intracellular Ca^{2+} release and SOCE (Agrawal et al., 2013;
74 Megha and Hasan, 2017; Shakiryanova et al., 2011). Genetic and cellular studies
75 identified neuromodulatory inputs and SOCE as an essential component for
76 maturation of neural circuits for flight (Pathak et al., 2015; Venkiteswaran and Hasan,
77 2009). A focus of this flight deficit lies in a group of central dopaminergic neurons (or
78 DANs) that include the PPL1 and PPM3 DANs (Liu et al. 2012) marked by *THD' GAL4,*
79 alternately referred to henceforth as flight promoting DANs (fpDANs). Among the
80 fpDANs some PPL1 DANs project to the γ2α'1 lobe of the Mushroom Body (MB; Mao
81 and Davis 2009) a dense region of neuropil in the insect central brain, that forms a
82 relay centre for flight (Sharma and Hasan, 2020). Axonal projections from Kenyon
83 cells (KC) carry sensory inputs (Cervantes-Sandoval et al., 2017; Tsao et al., 2018;
84 Yagi et al., 2016) and those from DANs carry internal state information (Mao and
85 Davis, 2009; Riemensperger et al., 2005; Zolin et al., 2021) to functional
86 compartments of the MB, where dopamine release modulates the KC and MB output
87 neuron synapse (MBONs; Aso et al. 2014). The KC-DAN-MBON tripartite synapse,
88 carries a dynamically updating representation of the motivational and behavioural
89 state of the animal (Aso and Rubin, 2016; Berry et al., 2015; Owald et al., 2015;
90 Waddell, 2016). Here we have investigated the molecular mechanisms that underlie
91 the ability of neuromodulatory acetylcholine signals, acting through SOCE during
92 circuit maturation, to determine fpDAN function required for *Drosophila* flight.
93

94 **Results**

95 **A spatio-temporal requirement for SOCE determines flight**

96 To understand how neuromodulator stimulated SOCE alters neuronal
97 properties over developmental time scales we began by refining further the existing
98 spatio-temporal coordinates of SOCE requirement for flight. Flight promoting
99 dopaminergic neurons (DANs) with a requirement for SOCE have been identified
100 earlier by expression of a dominant negative *Orai* transgene, which renders the
101 channel Ca^{2+} impermeable, thus abrogating all SOCE (*Orai*^{E180A}; Figure 1A; Pathak et
102 al. 2015; Yeromin et al. 2006). These include a smaller subset of *THD'GAL4* marked
103 DANs, where acetylcholine promotes dopamine release through the muscarinic
104 acetylcholine receptor (mAchR) by stimulating IP_3/Ca^{2+} signaling (Sharma and Hasan,
105 2020). *Orai*^{E180A} expression in a subset of 21-23 dopaminergic neurons marked by
106 *THD' GAL4* (Figure 1B) led to complete loss of flight (Figure 1C) while overexpression
107 of the wildtype *Orai* transgene had a relatively minor effect (Figure S1A).
108 *THD'* marks DANs in the PPL1, PPL2, and PPM3 clusters of the adult central
109 brain (Figure 1B) of which the PPL1 (10-12) and PPM3 (6-7) cell clusters constitute
110 the fpDANs (Pathak et al., 2015). Among these 16-19 DANs, two pairs of PPL1 DANs
111 projecting to the $\gamma 2\alpha'1$ lobes of the mushroom body (marked by the MB296B split
112 GAL4 driver and schematised in Figure S1B; Aso et al. 2014; Aso and Rubin 2016)
113 were identified as contributing to the flight deficit to a significant extent (Figures 1C;
114 S1C). The MB296B DANs form part of a central flight relay centre identified earlier as
115 requiring IP_3/Ca^{2+} signaling (Sharma and Hasan, 2020). That the *THD'* neurons are
116 required for flight was further confirmed by inhibiting their function. Acute activation of
117 either a temperature sensitive *Dynamin* mutant (*Shibire*^{ts}; Kitamoto 2001), which
118 blocks exocytosis at an elevated temperature, or acute expression of the tetanus toxin
119 light chain fragment (*TeTxLC* ; Sweeney et al. 1995) which cleaves *Synaptobrevin*, an
120 essential component of the synaptic release machinery in *THD'* neurons led to severe
121 flight defects (Figure S1D).
122 Previous work has demonstrated that intracellular Ca^{2+} release through the
123 IP_3R, that precedes SOCE (Figure 1A), is required during late pupal development in
124 *THD'* marked DANs for flight (Pathak et al., 2015; Sharma and Hasan, 2020). The
125 precise temporal requirement for SOCE in *THD'* neurons was investigated by inducing
126 *Orai*^{E180A} transgene expression for specific periods of pupal development and in adults
127 with the *tubulinGAL80*^{ts} based temperature sensitive expression system, (TARGET-

128 Temporal And Regional Gene Expression Targeting; McGuire et al., 2004).
129 Approximately 100 hours of pupal development were binned into 24 hour windows,
130 wherein SOCE was abrogated by *Orai*^{E180A} expression, following which, normal
131 development and growth was permitted. Flies were assayed for flight 5 days post
132 eclosion. Abrogation of SOCE by expression of the *Orai*^{E180A} dominant negative
133 transgene at 72 to 96 hrs after puparium formation (APF), resulted in complete loss of
134 flight as compared to minor flight deficits observed upon expression of *Orai*^{E180A} during
135 earlier developmental windows (Figure 1D). Abrogation of flight also occurred upon
136 *Orai*^{E180A} expression during the first 2 days post-eclosion (see discussion) whereas
137 abrogation of SOCE 5 days after eclosion as adults resulted in only modest flight
138 deficits (Figure 1D), indicating that SOCE is required for maturation of *THD'* marked
139 flight dopaminergic neurons. Earlier work has shown that loss of SOCE by expression
140 of *Orai*^{E180A} does not alter the number of dopaminergic neurons or affect neurite
141 projection patterns of PPL1 and PPM3 neurons (Pathak et al., 2015). Of these two
142 clusters, PPM3 DANs project to the ellipsoid body in the central complex (Kong et al.,
143 2010), and PPL1 DANs project to the mushroom body and the lateral horn (Mao and
144 Davis, 2009) and aid in the maintenance of extended flight bouts (Sharma and Hasan,
145 2020).
146
147 **Loss of SOCE in late pupae leads to a re-organisation of neuronal gene**
148 **expression**
149 The molecular consequences of loss of SOCE in *THD'* neurons were
150 investigated next by undertaking a comprehensive transcriptomic analysis from
151 fluorescence activated and sorted (FACS) *THD'* neurons with or without *Orai*^{E180A}
152 expression and marked with eGFP (Figure 1E; S1E). *THD'* neurons were obtained
153 from pupae at 72 ± 6h APF (essential SOCE requirement for flight; Figure 1E).
154 Expression analysis of RNAseq libraries generated from *THD'* neurons revealed a
155 reorganisation of the transcriptome upon loss of SOCE (Figure 1F). Expression of 822
156 genes was downregulated (with a fold change cut-off of < -1) as assessed using 3
157 different methods of Differentially Expressed Genes (DEG) analysis (Figure 1G)
158 whereas 137 genes were upregulated (Figure S1F). To understand if loss of SOCE
159 affects genes expressed in neurons from the pupal stage, we used the modEncode

160 dataset (Celniker et al., 2009; modENCODE Consortium et al., 2010) to reconstruct
161 developmental trajectories of all genes expressed in *THD'* neurons (Figure S1G).
162 Using an unsupervised clustering algorithm, we classified genes expressed in *THD'*
163 neurons into 3 clusters where 'Cluster 0' is low expression throughout development;
164 'Cluster 1' exhibits a larval peak in expression and 'Cluster 2' exhibits a pupal peak in
165 expression (Figure 1H). The majority of expressed genes (>95%) classify as low
166 expression throughout (Cluster 0) and were removed from further analysis. Genes
167 belonging to either the downregulated gene set or the upregulated gene set in SOCE-
168 deficient *THD'* neurons and a random set of genes were analysed further. A
169 comparison of the proportion of DEGs classified in the larval and pupal clusters
170 revealed that >75% of downregulated genes belonged to the pupal peak (Cluster 2)
171 whereas <20% of either the upregulated genes or a random set of genes classified as
172 belonging to the pupal peak (Figure 1I). Moreover, downregulated genes exhibit higher
173 baseline expression in wildtype pupal *THD'* neurons (Figures S1H, I). These analyses
174 suggest that SOCE induces expression of a set of genes in *THD'* neurons during the
175 late pupal phase which are subsequently required for flight. These are henceforth
176 referred to as SOCE-responsive genes.
177

178 **SOCE regulates gene expression through a balance of Histone 3 Lysine 36**
179 **trimethylation and Histone 3 Lysine 27 trimethylation**

180 Gene ontology (GO) analysis of SOCE-responsive genes revealed
181 'Transcription', 'Ion transporters', 'Ca^{2+} dependent exocytosis', 'GPCRs', 'Synaptic
182 components', and 'Kinases' as top GO categories (Figure 2A). Among these,
183 'Transcription' and 'Ion transporters' represented categories with the highest
184 enrichment. Further analysis of genes that classified under 'Transcription' revealed
185 SET domain containing genes that encode histone lysine methyltransferases
186 implicated in chromatin regulation and gene expression (Dillon et al., 2005) and
187 among the SET domain containing genes, *Set1* and *Set2* showed distinct
188 downregulation (Figure 2B). One of these genes, the H3K36me3 methyltransferase
189 *Set2* (Figure 2C), was identified in a previous RNAseq from larval neurons with loss
190 of IP_3R-mediated Ca^{2+} signaling (Mitra et al., 2020). RT-PCRs from sorted *THD'*
191 neurons confirmed that *Set2* levels are indeed downregulated (by 76%) in *THD'*

192 neurons expressing *Orai*^{E180A} and to the same extent as seen upon expression of
193 *Set2*^{RNAi} (79% downregulation; Figure 2C). *Set1* and *Set2* perform methyltransferase
194 activity at H3K4 and H3K36 histone residues respectively (Ardehali et al., 2011;
195 Stabell et al., 2007). Both these markers are epigenetic signatures for transcriptional
196 activation, where H3K4me3 is enriched at the 5' end of the gene body and H3K36me3
197 is enriched in the gene bodies of actively transcribed genes ; schematised in Figure
198 S2A). In the adult CNS, *Set2*, is expressed at 4-fold higher levels compared to *Set1*
199 (Figure S2B; modENCODE Consortium et al., 2010). *Set2* also shows a steep 5.5 fold
200 increase in expression levels during the pupal to adult transition, compared to a 2 fold
201 increase in *Set1* (Figure S2B). These observations coupled with the previous report of
202 Set2 function downstream of IP_3R/Ca^{2+} signaling in larval glutamatergic neurons(Mitra
203 et al., 2020), led us to pursue the role of Set2 in *THD'* neurons.
204 *Set2* encodes the only *Drosophila* methyltransferase which is specific for
205 H3K36 trimethylation (Stabell et al., 2007). To understand the functional significance,
206 if any, of down-regulation of *Set2* in *THD'* neurons upon loss of SOCE, four
207 independent *Set2* RNAi constructs were obtained. Knockdown of *Set2* in *THD'*
208 neurons with all four RNAi lines tested resulted in significant flight defects (Figure 2D;
209 S2C). *Set2* function for flight was additionally verified in the PPL1 DANs projecting to
210 the $\gamma 2\alpha'1$ lobe of the mushroom body (*MB296BGAL4*; Figure S2D). To test the
211 hypothesis that *Set2* expression and function for flight is regulated by SOCE, we
212 overexpressed *Set2* in the *Orai*^{E180A} background, using GAL4-UAS driven
213 heterologous *Set2*^{WT} expression or CRISPR-dCas9::VPR driven overexpression
214 (Gilbert et al., 2013) from the endogenous locus, and measured flight (Figure 2D data
215 in purple and brown). Flies expressing *Orai*^{E180A} in the *THD'* neurons, which are
216 flightless, exhibit significant rescue in flight bout durations upon *Set2* overexpression,
217 through either method (Figure 2D, compare red with purple and brown data), but not
218 upon expression of a control transgene, *GCamP6m* (Figure S2E, compare data in
219 green and red). Additionally, overexpression of a key SOCE component, the ER Ca^{2+}
220 sensor *STIM* in a *Set2*^{RNAi} background led to a rescue (Figure S2E, compare pink and
221 grey data). Excess STIM presumably drives higher SOCE sufficient to rescue flight
222 bout durations caused by deficient *Set2* levels. These two sets of data taken together
223 with downregulation of *Set2* upon expression of *Orai*^{E180A} (Figure 2C) support the

224 hypothesis that SOCE driven expression of *Set2* in fpDANs is required for flight. That
225 Set2 function downstream of SOCE, occurs specifically through its methyltransferase
226 activity was supported through experiments where knockdown of the demethylase
227 *Kdm4B*, the primary histone demethylase expressed in these neurons (Figure S2F),
228 rescued flight in *THD'>Orai*^{E180A} flies (Figure 2D; data in pink). Knockdown of the lower
229 expressed *Drosophila* H3K36 demethylase isoform, *Kdm4A,* did not show a similar
230 rescue (Figure S2G; data in pink). Moreover, both *Set2* depletion and loss of SOCE
231 (*THD'>Orai*^{E180A}) lead to a decrease in the normalised H3K36me3 signal in *THD'*
232 neurons (Figure 2E).

233 To understand if deficient H3K36me3 is found in the SOCE-responsive genes,
234 we quantified the enrichment of H3K36me3 at SOCE-responsive loci from an
235 H3K36me3 ChIP-Seq dataset (modENCODE Consortium et al., 2010) from wild-type
236 adult heads (Figure 2F). We observed an enrichment of the H3K36me3 signal over
237 the gene bodies of the SOCE-responsive genes (Figure 2F). Additionally, genes that
238 were more affected by loss of SOCE (greater extent of downregulation), had a
239 correspondingly higher H3K36me3 signal (Figure 2G) as compared with a random set
240 of genes (Figure 2G; data in grey), further indicating that one of the ways SOCE
241 regulates gene expression is through Set2 mediated deposition of H3K36me3.

242 The gene *E(z)* that encodes a component of the PRC2 complex (*EZH2*), which
243 deposits H3K27me3 is up-regulated upon loss of SOCE (Figure 2B) suggesting that
244 SOCE could affect additional histone modifications. While H3K36me3 is a marker for
245 transcriptional activation (Krogan et al., 2003), H3K27me3 is a repressive signature
246 which silences transcription (Cai et al., 2021). These two marks are antagonistic as
247 deduced from studies which have shown that deposition of H3K36me3 allosterically
248 inhibits the Polycomb Repressive Complex (PRC2), thereby preventing it from
249 depositing the H3K27me3 signature at the same genomic loci (Finogenova et al.,
250 2020). A comparison of H3K36me3 and H3K27me3 peaks over the 822 SOCE-
251 responsive genes revealed a higher enrichment of H3K36me3 versus H3K27me3 in
252 wild type fly heads (Figure 2H; modENCODE Consortium et al., 2010), suggesting that
253 robust expression of these genes in adult neurons occurs through a SOCE-dependent
254 mechanism initiated in late pupae (schematised in Figure 2I). To test this hypothesis,
255 we fed SOCE-deficient flies (*THD'GAL4>Orai*^{E180A}) GSK343, a pharmacological

256 inhibitor (Verma et al., 2012) of the EZH2 component of PRC2 that is known to reduce
257 H3K27me3 chromatin marks and performed flight assays. Feeding of GSK343 lead to
258 partial rescue of flight in *THD'> Orai*^{E180A} flies in a dose dependent manner with
259 maximal flight bout durations of up to 400 sec (Figure 2J; S2H).
260

261 **Normal cellular responses of PPL1 DANs require Orai mediated SOCE and**
262 **H3K36 trimethylation**

263 Next we investigated Ca^{2+} responses in SOCE and H3K36 trimethylation
264 deficient *THD'* PPL1 DANs upon stimulation with a neuromodulatory signal for the
265 muscarinic acetylcholine receptor (mAChR). It is known that *THD'* marked PPL1 DANs
266 receive cholinergic inputs that stimulate store Ca^{2+} release through the IP_3R, leading
267 to SOCE through Orai (Figure 3A; Ebihara et al., 2006; Sharma and Hasan, 2020). In
268 support of this idea, either expression of *Orai*^{E180A} or knockdown of the IP_3R attenuated
269 the response to carbachol (CCh), a mAChR agonist, in PPL1 DANs (Figure 3B-D;
270 Figure S3A-C). Importantly, knockdown of *Set2* also abrogated the Ca^{2+} response to
271 CCh (Figure 3B-D), whereas overexpression of a transgene encoding *Set2* in *THD'*
272 neurons either with loss of SOCE (*Orai*^{E180A}) or with knockdown of the IP_3R (*itpr*^{RNAi}),
273 lead to significant rescue of the Ca^{2+} response, indicating that *Set2* is required
274 downstream of SOCE (Figure 3B-D) and IP_3/Ca^{2+} signalling (Figure S3A-C).

275 An understanding of how Set2 might rescue cellular IP_3/Ca^{2+} signaling was
276 obtained in an earlier study where it was demonstrated that *Set2* participates in a
277 transcriptional feedback loop to control the expression of key upstream components
278 such as the *mAChR* and the *IP$_3$R* in a set of larval glutamatergic neurons (Mitra et al.,
279 2020). To test whether *Set2* acts through a similar transcriptional feedback loop in the
280 current context, *THD'* DANs were isolated using FACS from appropriate genetic
281 backgrounds and tested for expression of key genes required for IP_3/Ca^{2+} signaling
282 (*mAChR* and *itpr)* and SOCE (*Stim* and *Orai*). Loss of SOCE upon expression of
283 *Orai*^{E180A} lead to a significant decrease in the expression of *itpr (72%* downregulation;
284 Figure 3E*)*, *mAChR (56%* downregulation; Figure 3E*)*, *Stim (63%* downregulation;
285 Figure 3E) in *THD'* DANs. As expected *Orai* expression (Figure 3E) increased 2-fold
286 presumably due to overexpression of the *Orai*^{E180A} transgene. Importantly, knockdown
287 of *Set2* in *THD'* neurons also led to downregulation of *itpr* (43%), *mAChR* (78%) and

288 *Stim* (61%) (Figure 3E). Overexpression of *Set2* in the background of *Orai*^{E180A} led to
289 a rescue in the levels of *itpr* (69% increase), *mAChR* (43% increase), and *Stim* (40%
290 increase) (Figure 3E). Overexpression of *Set2* in wildtype *THD'* neurons resulted in
291 upregulation of *mAChR* and *Orai* (Figure 3E). These findings indicate that while SOCE
292 regulates *Set2* expression (Figure 2C), *Set2* in turn functions in a feedback loop to
293 regulate expression of key components of IP_3/Ca^{2+} and SOCE such as *mAchR, IP_3R,*
294 *STIM* and *Orai* (Figure 3E). Thus, ectopic *Set2* overexpression in SOCE deficient *THD'*
295 neurons, leads to increase in expression of key genes that facilitate intracellular Ca^{2+}
296 signalling and SOCE (schematised in Figure 3F).
297
298 **Trithorax-like or Trl is an SOCE responsive transcription factor in *THD'* DANs**
299 The data so far identify SOCE as a key developmental regulator of the neuronal
300 transcriptome in *THD'* marked DANs, where it upregulates Set2 expression and thus
301 enhances the activation mark of H3K36 trimethylation on specific chromatin regions.
302 However, the mechanism by which SOCE regulates expression of *Set2,* and other
303 relevant effector genes remained unresolved (Figure 3F). In mammalian T cells,
304 SOCE leads to de-phosphorylation of the NFAT (Nuclear Factor of Activated T-cells)
305 family of transcription factors by Ca^{2+}/Calmodulin sensitive phosphatase Calcineurin,
306 followed by their nuclear translocation and ultimately transcription of relevant target
307 genes (Hogan et al., 2003). Unlike mammals, the *Drosophila* genome encodes a
308 single member of the NFAT gene family, which does not possess calcineurin binding
309 sites, and is therefore insensitive to intracellular Ca^{2+} and SOCE (Keyser et al., 2007).
310 In order to identify transcription factors (TFs) that regulate SOCE-mediated
311 gene expression in *Drosophila* neurons, we examined the upstream regions (up to 10
312 kb) of SOCE-regulated genes using motif enrichment analysis (Zambelli et al., 2009)
313 for TF binding sites (Figure 4A). This analysis helped identify several putative TFs with
314 enriched binding sites in the regulatory regions of SOCE-regulated genes (Figure 4B,
315 S4A) which were then analyzed for developmental expression trajectories (Hu et al.,
316 2017) in the *Drosophila* CNS (Figure 4B; lower panel). Among the top 10 identified
317 TFs, the homeobox transcription factor Trl/GAF had the highest enrichment value,
318 lowest p-value (Figure 4B) and was consistently expressed in the CNS through all
319 developmental stages, with a distinct peak during pupal development (Figure 4B;

320 lower panel). To test the functional significance of Trl/GAF, we tested flight in flies with
321 *THD'* specific knockdown of *Trl* using two independent RNAi lines (Figure 4C) as well
322 as in existing *Trl* mutant combinations that were viable as adults (Figure S4B). In all
323 cases significant flight deficits were observed (Figure 4C, S4B). Moreover, the flight
324 deficits could be rescued by raising SOCE either directly through overexpression of
325 *STIM* or indirectly by *Set2* overexpression (Figure 4C; data in brown and pink
326 respectively).

327 To further test Trl function, as an effector of intracellular Ca^{2+} signaling and
328 SOCE, we investigated genetic interactions of $Trl^{13C,}$ a hypomorphic mutant *Trl* allele,
329 with an existing deficiency for the ER-Ca^{2+} sensor STIM ($STIM^{KO}$), an essential
330 activator of the Orai channel (Wang et al., 2010) as well as existing mutants for an
331 intracellular ER-Ca^{2+} release channel, the IP_3R (Joshi et al., 2004). While $STIM^{KO}/+$
332 flies demonstrate normal flight bout durations, adding a single copy of the Trl^{13C} allele
333 to the $STIM^{KO}$ heterozygotes (i.e., $STIM^{KO}/Trl^{13C}$ trans-heterozygotes) resulted in
334 significant flight deficits, which could be rescued by overexpression of *STIM* or *Set2*
335 (Figure 4D). A single copy of Trl^{13C} placed in combination with a single copy of various
336 *itpr* mutant alleles, also showed a significant reduction in the duration of flight bouts
337 (Figure S4C). Together these genetic data provide strong support for Trl as a SOCE-
338 responsive TF. Due to the strong flight deficit observed by expression of $Orai^{E180A}$ we
339 were unable to test genetic interactions of *Trl* with Orai directly. *Orai RNAi* strains
340 exhibit off-target effects and *Orai* hypomorphs are unavailable.

341 The requirement of *Trl* for SOCE-dependent gene expression was tested
342 directly by measuring *Set2* transcripts in *THD'* neurons with knockdown of *Trl*
343 ($THD'>Trl^{RNAi}$). *Set2* has 20 Trl binding sites in a 2 Kb region upstream of the
344 transcription start site (Figure S4D) and knockdown of *Trl* resulted in downregulation
345 of *Set2* (32%) and the Set2 regulated genes *itpr* (56%) and *mAchR* (73%; Figure 4E).
346 Moreover, a trans-heterozygotic combination of hypomorphic Trl alleles ($Trl^{13C/62}$) had
347 markedly reduced levels of brain H3K36me3 (Figure 4F).

348 To test if Trl drives cellular function in the fpDANs, we stimulated the mAChR
349 with CCh and measured Ca^{2+} responses in fpDANs with knockdown of *Trl*. Compared
350 to *WT* fpDANs, which respond robustly to cholinergic stimulation, Trl^{RNAi} expressing
351 DANs, exhibit strongly attenuated responses (Figure 4G-I). Overexpression of *Set2* in

352 the *Trl*^{RNAi} background rescued the cholinergic response (Figure 4G-I). The rescue of
353 both flight (Figure 4C, D) and the cholinergic response (Figure 4G-I) by overexpression
354 of *Set2* in flies with knockdown of *Trl* in *THD'* neurons (*THD'>Trl*^{RNAi}), confirms that Trl
355 acts upstream of *Set2* to ensure optimal neuronal function and flight.
356

357 **Trl function downstream of SOCE targets neuronal excitability through changes**
358 **in ion channel gene expression including VGCCs**

359 The results obtained so far indicate that Trl could function as an intermediary
360 transcription factor between SOCE and its downstream effector gene *Set2*.
361 Overexpression of *Trl*, however, is unable to rescue the loss of flight caused by loss
362 of SOCE (*THD'>Orai*^{E180A}; Figure 5A). Moreover, *Trl* transcript levels are unchanged
363 in the *Orai*^{E180A} condition (Figure 5B) suggesting that Trl requires Ca^{2+} influx through
364 SOCE for its function to go from an 'inactive' form to an 'active' form (schematized in
365 Figure 5C). Although Trl does not possess a defined Ca^{2+} binding domain, it has been
366 shown to interact with a diverse set of proteins (Lomaev et al., 2017) including Ca^{2+}
367 sensitive kinases, and is known to undergo phosphorylation (Zhai et al., 2008). These
368 data support a model (schematized in Figure 5C) wherein Ca^{2+} influx through SOCE
369 sustains Trl activation, leading to expression of *Set2*.

370 Next we investigated the extent to which the identified SOCE-Trl-Set2
371 mechanism impacts fpDAN function. 'Ion transport' is among the top GO terms
372 identified in SOCE-responsive genes (Figure 2A). Indeed, multiple classes of ion
373 channel genes including several $Na^{+,}$ K^{+} and Cl^{-} channels are downregulated in
374 fpDANs upon expression of *Orai*^{E180A} (Fig 5D, E). Regulation of ion channel gene
375 expression by Trl was indicated from the enrichment of Trl binding sites in regulatory
376 regions of some ion channel loci (Figure 5F). We purified fpDANs with knock down of
377 *Trl* (*THD'>Trl*$^{RNAi-1}$) and measured expression of a few key voltage-gated ion channel
378 genes (Fig 5F). *NaCP60E*, *para* (Na^{+} channels), *cac*, *ca-α1D* (VGCC subunits), *hk*,
379 and *eag* (outward rectifying K^{+} channels) are all downregulated between 0.6-0.9 fold
380 upon *Trl* knockdown (Fig 5G) as well as upon loss of SOCE (Fig 5B). Taken together,
381 these results indicate that the expression of key voltage-gated ion channel genes
382 which are required for the depolarization-mediated response, maintenance of

383 electrical excitability and neurotransmitter release is a focus of the transcriptional
384 program set in place by SOCE-Trl-Set2 .

385 To test the functional consequences of altered ion channel gene expression
386 downstream of Trl, neuronal activity of the fpDANs was tested by means of KCl-
387 evoked depolarisation. PPL1 DANs exhibited a robust Ca^{2+} response that was lost
388 upon knock down of *Trl* (Figure 5H-J; data in orange). In consonance with the earlier
389 behavioural experiments (Figure 5A), overexpression of Trl^{+} in *THD'* DANs did not
390 rescue the KCl response in PPL1 DANs with loss of SOCE ($OraiE^{180A}$; Trl^{OE}, Figure
391 5I, J), further reinforcing the hypothesis that, Trl activity in fpDANs is dependent of
392 Ca^{2+} entry through Orai.

393 Response to KCl is also lost in PPL1 neurons by knockdown of *Set2* and
394 restored to a significant extent by overexpression of *Set2* in *THD'* DANs lacking SOCE
395 ($Orai^{E180A}$;$Set2^{OE;}$ Figure 6A-C). We confirmed that the KCl response of PPL1 neurons
396 requires VGCC function, either by treatment with Nimodopine (Xu and Lipscombe,
397 2001), an L-type VGCC inhibitor or by knockdown of a conserved VGCC subunit *cac*
398 *(cac^{RNAi})*. Both forms of perturbation abrogated the depolarisation response to KCl in
399 PPL1 neurons (Figures 6D-F; data in purple or orange respectively). Moreover, the
400 Ca^{2+} entry upon KCl-mediated depolarization in PPL1 neurons is a cell-autonomous
401 property as evident by measuring the response after treatment with the Na^{+} channel
402 inhibitor, Tetrodotoxin (TTX; Figures 6D-F; data in magenta).

403 Having confirmed that the Ca^{2+} response towards KCl depolarisation requires
404 VGCCs, we tested the expression level of key components of *Drosophila* VGCCs
405 (Figure 6G) in *THD'* DANs, including *cacophony* (*cac*), *ca-α1D*, *ca-α1T*, and *ca-β*. All
406 four subunits of *Drosophila* VGCC are downregulated upon loss of SOCE ($Orai^{E180A}$;
407 Figure 6H) in *THD*' DANs whereas overexpression of *Set2* in the background of
408 $Orai^{E180A}$ restored expression of the four VGCC subunits tested (Figure 6H), thus
409 explaining recovery of the KCl response upon *Set2* overexpression in PPL1 neurons
410 lacking SOCE ($Orai^{E180A}$; Figures 6A-C).

411 The functional significance of downregulation of VGCC subunits by the SOCE-
412 Trl-Set2 pathway was tested directly by knockdown of the 4 VGCC subunits
413 independently in PPL1 neurons followed by measurement of flight bout durations.
414 Significant loss of flight was observed with knockdown of each subunit (Figure 6I)

415 though in no case was the phenotype as strong as what is observed with loss of SOCE
416 (*Orai*^{E180A}; Figure 1D). These data suggest that in addition to VGCC subunit
417 expression, appropriate expression of other ion channels in the fpDANs is of functional
418 significance. This idea is further supported by the observation that loss of flight upon
419 loss of SOCE cannot be restored by overexpression of *cac* alone (Figure 6J)
420 indicating that optimal neuronal activity requires an ensemble of genes, including ion
421 channels, whose expression is regulated by SOCE-Trl-Set2.
422

423 ***THD'* DANs require SOCE for developmental maturation of the neuronal**
424 **excitability threshold**

425 The functional relevance of changes in neuronal excitability during pupal
426 maturation of the PPL1-dependent flight circuit was tested next. Inhibition of *THD'*
427 DANs from 72 to 96 hours APF using acute induction of the inward rectifying K^+
428 channel *Kir2.1*(Johns et al., 1999) or optogenetic inhibition through the hyperpolarizing
429 Cl^- channel *GtACR2* (Govorunova et al., 2015) resulted in significant flight deficits
430 (Figure 7A; data in dark or light green). Similar flight defects were recapitulated upon
431 hyperactivation of *THD'* neurons through either optogenetic (*CsChrimson*; Klapoetke
432 et al., 2014) or thermogenetic (*TrpA1*; Viswanath et al., 2003) stimulation (Figure 7A;
433 data in orange or red), indicating that these neurons require balanced neuronal activity
434 during a critical window in late pupal development, failing which the flight circuit
435 malfunctions. To test if restoring excitability in fpDANs lacking SOCE *(THD'>Orai*^{E180A})
436 is sufficient to restore flight, we induced hyperexcitability by overexpressing *NachBac*
437 (Nitabach, 2006) a bacterial Na^+ channel. *NachBac* expression rescued both flight
438 (*THD'>Orai*^{E180A}; Figure 7B) and excitability (Figures 7C-E). A partial rescue of flight
439 was also obtained by optogenetic stimulation of neuronal activity through activation of
440 *THD'>Orai*^{E180A} DANs using *CsChrimson* either 72-79 hrs APF or 0-2 days post
441 eclosion (Figure 7E). In this case, flight rescues were accompanied by a
442 corresponding rescue of *CsChrimson* activation induced Ca^{2+} entry (Figures 7F, G).
443 Moreover inducing neuronal hyperactivation with indirect methods such as excess K^+
444 supplementation (Figure S7A) or impeding glial K^+ uptake, by genetic depletion of the
445 glial K^+ channel *sandman* (Weiss et al., 2019), partially rescued flight in animals
446 lacking SOCE in the *THD'* DANs (Figure S7B). Together, these results indicate that

447 SOCE, through Trl and Set2 activity, determines the threshold of fpDAN activation
448 during circuit maturation by regulating expression of voltage-gated ion channel genes,
449 like *cac.*

450 fpDANs also require a balance between H3K36me3/H3K27me3 mediated
451 epigenetic regulation (Figure 2K). To understand if this epigenetic balance affects
452 flight through modulation of neuronal excitability, we measured KCl-induced
453 depolarizing responses of PPL1 DANs in Orai deficient animals (*THD'>Orai*^{E180A}) fed
454 on the H3K27me3 antagonist GSK343 (0.5 mM). GSK343 fed animals were sorted
455 into 2 groups (Fliers/Non-Fliers) on the basis of flight bout durations of greater or lesser
456 than 30 s (Figure S7C), and tested for responses to KCl (Figures S7D, E).
457 *THD'>Orai*^{E180A} flies fed on GSK343 showed a rescue in KCl responses, with a clearly
458 enhanced response in the fliers compared to the non-fliers (Figures S7D, E), thereby
459 reiterating the hypothesis that SOCE-mediated regulation of activity in these neurons
460 acts through epigenetic regulation between opposing histone modifications.
461

462 ***THD'* DANs require SOCE-mediated gene expression for neuromodulatory**
463 **dopamine release in the mushroom body γ lobe**

464 Dopaminergic neurotransmission requires presynaptic voltage gated Ca^{2+}
465 channels (VGCCs; Brimblecombe et al., 2015), and has been implicated in the
466 maturation of intrinsic neuronal excitability during circuit formation (Lieberman et al.,
467 2018). A number of fpDANs send projections to the γ2α'1 lobe of the MB (Figure 8A).
468 We examined the consequences of loss of SOCE on CCh-evoked DA release at the
469 γ2α'1 region of the mushroom body (Figure 8B; red arrow). For this purpose we used
470 the dopamine sensor *GRAB-DA* (Sun et al., 2018). Loss of SOCE (*THD'>Orai*^{E180A})
471 attenuated DA release (Figures 8C, D), which could be partially rescued by
472 overexpression of *Set2*. Taken together these data identify an SOCE-dependent gene
473 regulation mechanism acting through the transcription factor Trl, and the histone
474 modifier Set2 for timely expression of genes that impact diverse aspects of neuronal
475 function including excitability and sustained neurotransmitter release (schematised in
476 Figure 8E).
477

478 **Discussion**

Over the course of development, neurons define an excitability set point within a dynamic range (Truszkowski and Aizenman, 2015), which stabilizes existing connections (Mayseless et al., 2023) and enables circuit maturation (Johnson-Venkatesh et al., 2015). In this study, we identify an essential role for the store-operated Ca^{2+} channel *Orai* in setting the excitability threshold of a subset of dopaminergic neurons central to a MB circuit for *Drosophila* flight. Orai-mediated Ca^{2+} entry, initiated by neuromodulatory acetylcholine signals, is required for amplification of a signalling cascade, that begins by activation of the homeo-box transcription factor Trl, followed by upregulation of several genes, including *Set2*, a gene that encodes an enzyme for an activating epigenetic mark, H3K36me3. Set2 in turn establishes a transcriptional feedback loop to drive expression of key neuronal signaling genes, including a repertoire of voltage-gated ion channel genes required for neuronal activity in mature PPL1 dopaminergic neurons.

SOCE supports gene expression transitions during critical developmental windows

Studies in the *Drosophila* mushroom body have identified spontaneous bouts of voltage-gated Ca^{2+} channel mediated neuronal activity, through as yet unknown mechanisms, which occur during early adulthood driving refinement and maturation of behaviours such as associative learning (Leinwand and Scott, 2021). Our studies here, on a subset of 21-23 central dopaminergic neurons (Figures 1B, C) of which some send projections to the mushroom body and regulate flight behaviour, provide a mechanistic explanation for neuromodulation-dependent intracellular signaling culminating in transcriptional maturation of a circuit supporting adult flight. In the critical developmental window of 72-96 hrs APF, a cohort of SOCE-responsive genes, that include a range of ion channels, undergo a wave of induction. Loss of SOCE at this stage thus renders these neurons functionally incompetent (Figures 3B-D, 6G-I, 7D-F) and abrogates flight (Figure 1D). Developmentally assembled neuronal circuits require experience/activity-dependent maturation (Akin and Zipursky, 2020). The requirement of SOCE for flight circuit function during the early post eclosion phase (0-2 days) suggests that maturation of the flight circuit extends into early adulthood, where presumably feedback from circuit activity may further refine synaptic strengths

511 (Sugie et al., 2018). Expression of *Orai*^{E180A} in 5 day old adults had no effect on flight
512 (Figure 1E), indicating that either SOCE is not required for maintaining gene
513 expression in adults or that wildtype Orai channel proteins from late pupal and early
514 adults perdure for long periods. The absence of any visible changes to neurite
515 patterning suggest that SOCE in the MB-DANs works primarily to refine synaptic
516 function. In summary, our findings here identify Orai-driven Ca^{2+} entry as a key
517 signaling step for driving coordinated gene expression enabling the maturation of
518 nascent neuronal circuits and sustenance of adult behaviour.
519
520 **SOCE regulates a balance between competing epigenetic signatures**
521 Chromatin structure and function is dynamic over the course of brain
522 development (Kishi and Gotoh, 2018). One way neurons achieve dynamic spatio-
523 temporal control over developmental gene expression is via epigenetic mechanisms
524 such as post translational histone modifications (Geng et al., 2021). Cells possess an
525 extensive toolkit of histone modifiers, with characterised effects on transcriptional
526 output by either activating or repressing gene expression (Bannister and Kouzarides,
527 2011). However, relatively little, is known about how modifiers of histone marks are in
528 turn regulated to bring about the requisite changes in neuronal gene expression over
529 developmental timescales.
530 The SET-domain containing family of histone modifiers (Figure 2B), including
531 H3K36me3 methyltransferase Set2 (Figure 2C), identified here appear to function as
532 key transcriptional effectors induced downstream of neuromodulatory inputs that
533 stimulate Store-operated Ca^{2+} entry through Orai during pupal and adult maturation of
534 flight promoting dopaminergic neurons. SOCE-driven *Set2*-mediated H3K36me3
535 enhances the expression of key GPCRS, components of intracellular Ca^{2+} signaling
536 (Figure 2A) and ion channels (Figures 6A, B) for optimal dopaminergic neuron function
537 (Figure 7D-F) and flight (Figure 1C). Rescue of flight by genetic depletion of an
538 epigenetic 'eraser' *Kdm4B*, an H3K36me3 demethylase (Figure 2D) suggests that a
539 balance between perdurance of H3K36me3 and its removal is actively maintained on
540 the expressed genes. Interestingly, another member of the SET domain family, *E(z)*
541 is up-regulated upon loss of SOCE (Figure 2B). *E(z)* is a component of the *Drosophila*
542 PRC2 complex (Polycomb repressive complex), which represses gene expression

543 through H2K27me3 (Margueron and Reinberg, 2011). Structural studies on
544 *Drosophila* nucleosomes have elucidated that the H3K36me3 modification
545 allosterically inhibits the PRC2 complex activity (Finogenova et al., 2020). Our findings
546 support a model wherein at key developmental stages, SOCE determines the level of
547 these competing epigenetic signatures thus allowing gene expression by enhancing
548 Set2 mediated H3K36me3 (Fig 2H). Loss of SOCE leads to deficient Set2-mediated
549 H3K36me3 (Figure 2E), a likely shifting of the balance in favour of PRC2 mediated
550 H3K27me3 and overall repression in gene expression (as observed in Fig S1H, I).
551 Feeding SOCE-deficient animals a pharmacological inhibitor of PRC2 (GSK434) led
552 to a significant rescue in behaviour (Figure 2J) presumably by disinhibition of
553 H3K27me3 mediated gene repression. Though flight initiation is rescued in a dose
554 dependent manner, the duration of flight bouts is not sustained (Figure S2H) indicating
555 that suppression of H3K27me3 marks in the SOCE-deficient flies is partial. Our
556 findings indicate additional roles for other histone modifications such as Set1 mediated
557 H3K4me3, which may work in concert to regulate developmental gene expression
558 programs stimulated by SOCE. Future studies directed at a comprehensive
559 cataloguing of multiple epigenetic signatures in defined neuronal subsets using cell-
560 specific techniques should help elucidate these mechanisms.
561
562 **Trl as an SOCE responsive transcription factor**
563 SOCE-mediated regulation of gene expression has been reported in
564 mammalian neural progenitor cells (Somasundaram et al., 2014) and *Drosophila* pupal
565 neurons (Pathak et al., 2015; Richhariya et al., 2017), through as yet unknown
566 mechanisms. A combination of motif enrichment analysis over regulatory regions of
567 SOCE-responsive genes and expression enrichment analysis in cells of interest,
568 helped generate a list of putative SOCE-responsive transcription factors (Figure 4A,
569 B). Among these we experimentally validated Trl/Trithorax-like/GAGA factor as a
570 transcription factor required for maturation of excitability in flight promoting
571 dopaminergic neurons (Figure 4). Although Trl function has been reported in the
572 context of early embryonic development, where it has been implicated in zygotic
573 genome activation (Gaskill et al., 2021) (ZGA), expression of *Hox* genes (Shimojima,
574 2003), dosage compensation (Greenberg et al., 2004), and expression of a *Drosophila*

575 voltage-gated calcium channel subunit in germ cell development (Dorogova et al.,
576 2014), his is the first ever report of its role in regulating neuronal gene expression in
577 the context of SOCE and circuit maturation.

578 In vitro studies on *Drosophila* Trl reveal that it utilizes a Q-rich intrinsically
579 disordered domain (IDD) to self-multimerize or interact with a wide range of accessory
580 proteins (Wilkins and Lis, 1999). Multimeric complexes of Trl reside on chromatin with
581 an exceptionally long residence time and maintain chromatin in an 'open' state (Tang
582 et al., 2022). Trl has also been reported to directly interact with components of the
583 Transcription initiation and elongation complex (Chopra et al., 2008; Li et al., 2013),
584 support long distance promoter-enhancer interactions (Mahmoudi, 2003), mediate
585 active ATP-dependent chromatin remodeling by maintaining nucleosome free
586 stretches (Tsukiyama et al., 1994), and regulating global gene expression by
587 controlling transcriptional stalling and pausing (Tsai et al., 2016). SOCE-dependent
588 gene regulation may rely upon multiple transcription factors acting in concert in a cell
589 type and developmental stage specific contexts, of which Trl may be just one. Future
590 studies directed at other possible transcription factors downstream of SOCE would be
591 of interest.

592

593 **SOCE and the control of neuronal excitability and cholinergic neuromodulation**
594 **of a tripartite synapse in the mushroom body**

595 Neurons undergo maturation of their electrical properties with a gradual
596 increase in depolarizing responses and synaptic transmission over the course of pupal
597 development (Jarvilehto and Finell, 1983). Here we show that a subset of
598 dopaminergic neurons require a balance of ion channels for optimal excitation and
599 inhibition essential for adult function. Neuromodulatory signals, such as acetylcholine
600 are essential for acquiring this balance and act via an SOCE-Trl-Set2 mechanism
601 during late pupal and early adult stages. The ability of *Set2* overexpression to rescue
602 SOCE-deficient phenotypes (Figures 6A-C) indicates that anomalous gene expression
603 is the underlying basis of this phenotype. Indeed, SOCE deficient dopaminergic
604 neurons show reduced expression of an ensemble of voltage-gated ion channel genes
605 (Figures 5E, F). including genes encoding the outward rectifying K^+ channel *shaw*,
606 slow-inactivating voltage gated K^+ channel *shaker*, a Ca^{2+} gated K^+ channel *slowpoke*

607 and *cacophony* a subunit of the voltage gated Ca^{2+} channel (Figure 6G). Ion channels
608 like *Shaker* and *slowpoke* play an important role in establishing resting membrane
609 potential (Singh and Wu, 1990), neuronal repolarisation (Lichtinghagen et al., 1990)
610 and mediating afterhyperpolarisation (AHP) after repeated bouts of activity (Ping et
611 al., 2011). Though dopaminergic neurons require *Set2* mediated expression of
612 *cacophony* for excitability, *cacophony* is in itself insufficient to rescue the loss in
613 excitability and flight deficits upon loss of SOCE (Figure 6J). Both flight and KCl-
614 depolarisation in SOCE-deficient neurons could, however, be rescued by expression
615 of a heterologous depolarisation activated Na^{+} channel NachBac (Nitabach, 2006)
616 (Figures 7B-D), which increases neuronal excitability by stimulating a low threshold
617 positive feedback loop and to a lesser extent by CsChrimson-mediated optogenetic
618 induction of neuronal activity (Figure 7E). The poorer rescue by optogenetic activation
619 may stem from the fact that sustained bursts of activity are non-physiological and can
620 deplete the readily releasable pool of neurotransmitters (Arrigoni and Saper, 2014;
621 Kaeser and Regehr, 2017). Other indirect forms of inducing neuronal hyperactivation
622 (Figures S7A, B) in SOCE-deficient neurons also achieved minor rescues in flight.
623 These results identify SOCE as a key driver downstream of developmentally salient
624 neuromodulatory signals for expression of an ion channels suite that enables
625 generation of intrinsic electrical properties and functional maturation of the PPL1
626 DANs, and the flight circuit.
627
628 **Methods**
629
630 **Fly maintenance**
631 *Drosophila* strains were grown on standard cornmeal medium consisting of 80 g corn
632 flour, 20 g glucose, 40 g sugar, 15 g yeast extract, 4 ml propionic acid, 5 ml p-
633 hydroxybenzoic acid methyl ester in ethanol and 5 ml ortho-butyric acid in a total
634 volume of 1 l (ND) at 25°C under a light-dark cycle of 12 h and 12 h. Canton S was
635 used as wild type throughout. Mixed sex populations were used for all experiments.
636 Several fly stocks used in this study were sourced using FlyBase (https://flybase.org),
637 which is supported by a grant from the National Human Genome Research Institute at
638 the US National Institutes of Health (#U41 HG000739), the British Medical Research
639 Council (#MR/N030117/1) and FlyBase users from across the world. The stocks were

640 obtained from the Bloomington Drosophila Stock Centre (BDSC) supported by NIH
641 P40OD018537. All fly stocks used and their sources are listed in Supplementary Table
642 1.
643
644 **Flight Assays**
645 Flight assays were performed as previously described (Manjila and Hasan, 2018).
646 Briefly, flies aged 3–5 days of either sex were tested in batches of 8–10 flies, and a
647 minimum of 30 flies were tested for each genotype. Adult flies were anaesthetized on
648 ice for 2–3 min and then tethered between at the head-thorax junction using a thin
649 metal wire and nail polish. Post recovery at room temperature for 2-3 min, an air puff
650 was provided as stimulus to initiate flight. Flight duration was recorded for each fly for
651 15 min. For all control genotypes, GAL4 or UAS strains were crossed to the Wild Type
652 strain, *Canton S*. Flight assays are represented in the form of a swarm plot, wherein
653 each dot represents a flight bout duration for a single fly. The colours indicate different
654 genotypes. The Δ Flight parameter refers to the mean difference for comparisons
655 against the shared CS control which is shown as a Cumming estimation plot(Ho et al.,
656 2018). On the lower axes, mean differences are plotted as bootstrap sampling
657 distributions. Each mean difference is depicted as a dot. Each 95% confidence interval
658 is indicated by the ends of the vertical error bars. Letters beneath each distribution
659 refer to statistically indistinguishable groups after performing a Kruskall-Wallis test
660 followed by a post hoc Mann-Whitney U-test ($p<0.05$).
661
662 **FACS**
663 Fluorescence-activated cell sorting (FACS) was used to enrich eGFP labelled DANs
664 from pupal/adult. The following genotypes were used for sorting: wild type
665 *(THD'GAL4> UAS-eGFP), Orai^{E180A} (THD'GAL4> Orai^{E180A})*, Set2^{IR-1} *(THD'GAL4>*
666 *Set2^{IR-1})*, *Orai^{E180A}; Set2^{OE} (THD'GAL4> Orai^{E180A}; Set2^{OE}), Set2^{OE} (THD'GAL4>*
667 *Set2^{OE}), Trl^{IR-1} (THD'GAL4> Trl^{IR-1})*. Approximately 100 pupae per sample were
668 washed in 1×PBS and 70% ethanol. Pupal/adult CNSs were dissected in Schneider's
669 medium (ThermoFisher Scientific) supplemented with 10% fetal bovine serum, 2%
670 PenStrep, 0.02 mM insulin, 20 mM glutamine and 0.04 mg/ml glutathione. Post
671 dissection, the CNSs were treated with an enzyme solution [0.75 g/l Collagenase and
672 0.4 g/l Dispase in Rinaldini's solution (8 mg/ml NaCl, 0.2 mg/ml KCl, 0.05 mg/ml

673 NaH2PO4, 1 mg/ml NaHCO3 and 0.1 mg/ml glucose)] at room temperature for 30 min.
674 They were then washed and resuspended in ice-cold Schneider's medium and gently
675 triturated several times using a pipette tip to obtain a single-cell suspension. This
676 suspension was then passed through a 40 mm mesh filter to remove clumps and kept
677 on ice until sorting (less than 1 h). Flow cytometry was performed on a FACS Aria
678 Fusion cell sorter (BD Biosciences) with a 100 mm nozzle at 60 psi. The threshold for
679 GFP-positive cells was set using dissociated neurons from a non GFP-expressing
680 wild-type strain (*Canton S*). The same gating parameters were used to sort other
681 genotypes in the experiment. GFP-positive cells were collected directly in TRIzol and
682 then frozen immediately in dry ice until further processing. Details for all reagents used
683 are listed in Supplementary Table 2.
684
685 **RNA-Seq**
686 RNA from at least 600 sorted *THD'* DANs from the relevant genotypes, expressing
687 *UAS-eGFP* was subjected to 14 cycles of PCR amplification (SMARTer Seq V4 Ultra
688 Low Input RNA Kit; Takara Bio). 1 ng of amplified RNA was used to prepare cDNA
689 libraries (Nextera XT DNA library preparation kit; Illumina). cDNA libraries for 4
690 biological replicates for both control (*THD'GAL4/+*) and experimental
691 (*THD'GAL4>UAS-Orai*^{E180A}) genotypes were run on a Hiseq2500 platform. 50-70
692 million unpaired sequencing reads per sample were aligned to the dm6 release of the
693 *Drosophila* genome using HISAT2(Kim et al., 2015, 2019) and an overall alignment
694 rate of 95.2-96.8% was obtained for all samples. Featurecounts(Liao et al., 2014) was
695 used to assign the mapped sequence reads to the genome and obtain read counts.
696 Differential expression analysis was performed using three independent methods:
697 DESeq2(Love et al., 2014), limma-voom(Ritchie et al., 2015), and edgeR(Robinson et
698 al., 2009). A fold change cutoff of a minimum twofold change was used. Significance
699 cutoff was set at an FDR-corrected P value of 0.05 for DESeq2 and edgeR.
700 Volcanoplots were generated using VolcaNoseR (https://huygens.science.uva.nl/).
701 Comparison of gene lists and generation of Venn diagrams was performed using
702 Whitehead BaRC public tools (http://jura.wi.mit.edu/bioc/tools/). Gene ontology
703 analysis for molecular function was performed using DAVID(Huang et al., 2008, 2009).
704 Developmental gene expression levels were measured for downregulated genes

705 using FlyBase(Larkin et al., 2020) and DGET(Hu et al., 2017)
706 (www.flyrnai.org/tools/dget/web/), and were plotted as a heatmap using ClustVis
707 (Metsalu and Vilo, 2015) (https://biit.cs.ut.ee/clustvis/).
708
709 **qRT-PCRs**
710 Central nervous systems (CNSs) of the appropriate genotype and age were dissected
711 in 1× phosphate-buffered saline (PBS; 137 mM NaCl, 2.7 mM KCl, 10 mM Na_2HPO_4
712 and 1.8 mM KH_2PO_4) prepared in double distilled water treated with DEPC. Each
713 sample consisted of five CNS homogenized in 500 µl of TRIzol (Ambion,
714 ThermoFisher Scientific) per sample. At least three biological replicate samples were
715 made for each genotype. After homogenization the sample was kept on ice and either
716 processed further within 30 min or stored at −80°C for up to 4 weeks before
717 processing. RNA was isolated following the manufacturer's protocol. Purity of the
718 isolated RNA was estimated by NanoDrop spectrophotometer (ThermoFisher
719 Scientific) and integrity was checked by running it on a 1% Tris-EDTA agarose gel.
720 Approximately 100 ng of total RNA was used per sample for cDNA synthesis. DNAse
721 treatment and first-strand synthesis were performed as described previously(Pathak
722 et al., 2015). Quantitative real time PCRs (qPCRs) were performed in a total volume
723 of 10 µl with Kapa SYBR Fast qPCR kit (KAPA Biosystems) on an ABI 7500 fast
724 machine operated with ABI 7500 software (Applied Biosystems). Technical duplicates
725 were performed for each qPCR reaction. The fold change of gene expression in any
726 experimental condition relative to wild type was calculated as $2^{-\Delta\Delta Ct}$, where $\Delta\Delta C_t$=[C_t
727 (target gene) –C_t (rp49)] Expt. – [C_t (target gene) – C_t (rp49)]. Primers specific for rp49
728 and ac5c were used as internal controls. Sequences of all primers used are provided
729 in Supplementary Table 3.
730
731 **Functional imaging**
732 Adult brains were dissected in adult hemolymph-like saline (AHL: 108 mM NaCl, 5
733 mM KCl, 2 mM CaCl2, 8.2 mM $MgCl_2$, 4 mM $NaHCO_3$, 1 mM NaH_2PO_4, 5 mM
734 Trehalose, 10 mM Sucrose, 5 mM Tris, pH 7.5) after embedded in a drop of 0.1%
735 low-melting agarose (Invitrogen). Embedded brains were bathed in AHL and then
736 subjected to functional imaging. The genetically encoded calcium sensor
737 *GCaMP6m*(Chen et al., 2013) was used to record changes in intracellular cytosolic

738 Ca^{2+} in response to stimulation with carbachol or KCl. The GRAB-DA sensor(Sun et
739 al., 2018) was used to measure evoked dopamine release. Images were taken as a
740 time series on a xy plane at an interval of 1 s using a 20× objective with an NA of 0.7
741 on an Olympus FV3000 inverted confocal microscope. A 488 nm laser line was used
742 to record GCaMP6m / GRAB-DA measurements. All live-imaging experiments were
743 performed with at least 10 independent brain preparations. For measuring evoked
744 responses, KCl/Carbachol, was added on top of the samples. For optogenetics
745 experiments, flies were reared on medium supplemented with 200 μM ATR (all trans
746 retinal), following which neuronal activation was achieved using a 633-nm laser line
747 to stimulate *CsChrimson*(Klapoetke et al., 2014) while simultaneously acquiring
748 images with the 488 nm laser line, and the images were acquired every 1 s. The raw
749 images were extracted using FIJI(Schindelin et al., 2012) (based on ImageJ version
750 2.1.0/1.53c). ΔF/F was calculated from selected regions of interest (ROIs) using the
751 formula ΔF/F=(Ft-F0)/F0, where Ft is the fluorescence at time t and F0 is baseline
752 fluorescence corresponding to the average fluorescence over the first 40-time
753 frames. Mean ΔF/F time-lapses were plotted using PlotTwist(Goedhart, 2020)
754 (https://huygens.science.uva.nl/PlotTwist/). A shaded error bar around the mean
755 indicates the 95% confidence interval for CCh (50 μM) or KCl (70 mM) responses.
756 Peaks for individual cellular responses for each genotype was calculated from before
757 or after the point of stimulation, using Microsoft Excel and plotted as a paired plot
758 using SuperPlotsOfData(Goedhart, 2021)
759 (https://huygens.science.uva.nl/SuperPlotsOfData/).
760 Boxplots were plotted using PlotsOfData (Postma and Goedhart, 2019)
761 (https://huygens.science.uva.nl/PlotsOfData/).
762

763 **Immunohistochemistry**

764 Immunostaining of larval *Drosophila* brains was performed as described
765 previously(Daniels et al., 2008). Briefly, adult brains were dissected in 1x phosphate
766 buffered saline (PBS) and fixed with 4% Paraformaldehyde. The dissected brains were
767 washed 3-4 times with 0.2% phosphate buffer, pH 7.2 containing 0.2% Triton-X 100
768 (PTX) and blocked with 0.2% PTX containing 5% normal goat serum (NGS) for 2 hours
769 at room temperature. Respective primary antibodies were incubated overnight (14–16
770 hr) at 4°C. After washing 3-4 times with 0.2% PTX at room temperature, they were

771 incubated in the respective secondary antibodies for 2 hr at room temperature. The
772 following primary antibodies were used: chick anti-GFP antibody (1:10,000; A6455,
773 Life Technologies), mouse anti-nc82 (anti-brp) antibody (1:50), rabbit anti-H3K36me3,
774 mouse anti-RFP. Secondary antibodies were used at a dilution of 1:400 as follows:
775 anti-rabbit Alexa Fluor 488 (#A11008, Life Technologies), anti-mouse Alexa Fluor 488
776 (#A11001, Life Technologies). Confocal images were obtained on the Olympus
777 Confocal FV1000 microscope (Olympus) with a 40x, 1.3 NA objective or with a 60x,
778 1.4 NA objective. Images were visualized using either the FV10-ASW 4.0 viewer
779 (Olympus) or Fiji(Schindelin et al., 2012). Details for all reagents used are listed in
780 Supplementary Table 2.
781
782 **Western Blotting**
783 Adult CNSs of appropriate genotypes were dissected in ice-cold PBS. Between 5 and
784 10 brains were homogenized in 50 µl of NETN buffer [100 mM NaCl, 20 mM Tris-Cl
785 (pH 8.0), 0.5 mM EDTA, 0.5% Triton-X-100, 1× Protease inhibitor cocktail (Roche)].
786 The homogenate (10-15 µl) was run on an 8% SDS-polyacrylamide gel. The protein
787 was transferred to a PVDF membrane by standard semi-dry transfer protocols (10 V
788 for 10 min). The membrane was incubated in the primary antibody overnight at 4°C.
789 Primary antibodies were used at the following dilutions: rabbit anti-H3K36me3
790 (1:5000, Abcam, ab9050) and rabbit anti-H3 (1:5000, Abcam, ab12079). Secondary
791 antibodies conjugated with horseradish peroxidase were used at dilution of 1:3000
792 (anti-rabbit HRP; 32260, Thermo Scientific). Protein was detected by a
793 chemiluminescent reaction (WesternBright ECL, Advansta K12045-20). Blots were
794 first probed for H3K36me3, stripped with a solution of 3% glacial acetic acid for 10
795 min, followed by re-probing with the anti-H3 antibody.
796
797 **In silico ChIP-Seq Analysis**
798 H3K36me3 enrichment data was obtained from a ChIP-chip dataset (ID_301)
799 generated in *Drosophila* ML-DmBG3-c2 cells submitted to modEncode(Celniker et al.,
800 2009; modENCODE Consortium et al., 2010). Enrichment scores for genomic regions
801 were calculated using 'computematrix' and plotted as a tag density plot using
802 'plotHeatmap' from deeptools2(Ramírez et al., 2016). All genes were scaled to 2 kb
803 with a flanking region of 250 bp on either end. A 50 bp length of non-overlapping bins

804 was used for averaging the score over each region length. Genes were sorted based
805 on mean enrichment scores and displayed on the heatmap in descending order.
806
807 **Statistical tests**
808 Non-parametric tests were employed to test significance for data that did not follow a
809 normal distribution. Significant differences between experimental genotypes and
810 relevant controls were tested either with the Kruskal-Wallis test followed by Dunn's
811 multiple comparison test (for multiple comparisons) or with Mann-Whitney U tests (for
812 pairwise comparisons). Data with normal distribution were tested by the Student's T-
813 test. Statistical tests and p-values are mentioned in each figure legend. For calculation
814 and representation of effect size, estimationstats.com was used.
815

816 **Acknowledgements**

817 We acknowledge the Central Imaging and Flow Cytometry Facility (CIFF, NCBS) for
818 maintenance of microscopes and the *Drosophila* facility (Flyfacility, NCBS) for Fly
819 stock maintenance and development of transgenics.

820

821 **Competing Interests**

822 The authors declare no competing interests

823 **Funding**

824 This work was funded by grant No. BT/PR28450/MED/122/166/2018 from the
825 Department of Biotechnology, Govt. of India and core support by NCBS, TIFR. RM
826 and SR received graduate student fellowships from NCBS, TIFR.

827 **Data availability**

828 The RNA Sequencing data has been submitted to GEO under accession number
829 GSE230134.

830

References

Agrawal, T., Sadaf, S., & Hasan, G. (2013). A Genetic RNAi Screen for IP3/Ca2+ Coupled GPCRs in Drosophila Identifies the PdfR as a Regulator of Insect Flight. *PLoS Genetics*, *9*, e1003849. https://doi.org/10.1371/journal.pgen.1003849

Akin, O., & Zipursky, S. L. (2020). Activity regulates brain development in the fly. *Current Opinion in Genetics & Development*, *65*, 8–13. https://doi.org/10.1016/j.gde.2020.04.005

Ardehali, M. B., Mei, A., Zobeck, K. L., Caron, M., Lis, J. T., & Kusch, T. (2011). *Drosophila*Set1 is the major histone H3 lysine 4 trimethyltransferase with role in transcription. *The EMBO Journal*, *30*, 2817–2828. https://doi.org/10.1038/emboj.2011.194

Arrigoni, E., & Saper, C. B. (2014). What optogenetic stimulation is telling us (and failing to tell us) about fast neurotransmitters and neuromodulators in brain circuits for wake–sleep regulation. *Current Opinion in Neurobiology*, *29*, 165–171. https://doi.org/10.1016/j.conb.2014.07.016

Aso, Y., Hattori, D., Yu, Y., Johnston, R. M., Iyer, N. A., Ngo, T.-T. B., Dionne, H., Abbott, L. F., Axel, R., Tanimoto, H., & Rubin, G. M. (2014). The neuronal architecture of the mushroom body provides a logic for associative learning. *ELife*, *3*, e04577. https://doi.org/10.7554/eLife.04577

Aso, Y., & Rubin, G. M. (2016). Dopaminergic neurons write and update memories with cell-type-specific rules. *ELife*, *5*. https://doi.org/10.7554/eLife.16135

Bannister, A. J., & Kouzarides, T. (2011). Regulation of Chromatin by Histone Modifications. *Cell Research*, *21*, 381–395. https://doi.org/10.1038/cr.2011.22

Berry, J. A., Cervantes-Sandoval, I., Chakraborty, M., & Davis, R. L. (2015). Sleep Facilitates Memory by Blocking Dopamine Neuron-Mediated Forgetting. *Cell*, *161*, 1656–1667. https://doi.org/10.1016/j.cell.2015.05.027

Brimblecombe, K. R., Gracie, C. J., Platt, N. J., & Cragg, S. J. (2015). Gating of dopamine transmission by calcium and axonal N-, Q-, T- and L-type voltage-gated calcium channels differs between striatal domains. *The Journal of Physiology*, *593*, 929–946. https://doi.org/10.1113/jphysiol.2014.285890

Cai, Y., Zhang, Y., Loh, Y. P., Tng, J. Q., Lim, M. C., Cao, Z., Raju, A., Lieberman

863 Aiden, E., Li, S., Manikandan, L., Tergaonkar, V., Tucker-Kellogg, G., &
864 Fullwood, M. J. (2021). H3K27me3-rich genomic regions can function as
865 silencers to repress gene expression via chromatin interactions. *Nature*
866 *Communications*, *12*. https://doi.org/10.1038/s41467-021-20940-y
867 Celniker, S. E., Dillon, L. A. L., Gerstein, M. B., Gunsalus, K. C., Henikoff, S.,
868 Karpen, G. H., Kellis, M., Lai, E. C., Lieb, J. D., MacAlpine, D. M., Micklem, G.,
869 Piano, F., Snyder, M., Stein, L., White, K. P., & Waterston, R. H. (2009).
870 Unlocking the secrets of the genome. *Nature*, *459*(7249), 927–930.
871 https://doi.org/10.1038/459927a
872 Cervantes-Sandoval, I., Phan, A., Chakraborty, M., & Davis, R. L. (2017). Reciprocal
873 synapses between mushroom body and dopamine neurons form a positive
874 feedback loop required for learning. *ELife*, *6*. https://doi.org/10.7554/elife.23789
875 Chen, T.-W., Wardill, T. J., Sun, Y., Pulver, S. R., Renninger, S. L., Baohan, A.,
876 Schreiter, E. R., Kerr, R. A., Orger, M. B., Jayaraman, V., Looger, L. L.,
877 Svoboda, K., & Kim, D. S. (2013). Ultrasensitive fluorescent proteins for imaging
878 neuronal activity. *Nature*, *499*, 295–300. https://doi.org/10.1038/nature12354
879 Chopra, V. S., Srinivasan, A., Kumar, R. P., Mishra, K., Basquin, D., Docquier, M.,
880 Seum, C., Pauli, D., & Mishra, R. K. (2008). Transcriptional activation by GAGA
881 factor is through its direct interaction with dmTAF3. *Developmental Biology*, *317*,
882 660–670. https://doi.org/10.1016/j.ydbio.2008.02.008
883 Ciceri, G., Cho, H., Kshirsagar, M., Baggiolini, A., Aromolaran, K. A., Walsh, R. M.,
884 Goldstein, P. A., Koche, R. P., Leslie, C. S., & Studer, L. (2022). An epigenetic
885 barrier sets the timing of human neuronal maturation. *BioArxiv*.
886 https://doi.org/10.1101/2022.06.02.490114
887 Daniels, R. W., Gelfand, M. V, Collins, C. A., & DiAntonio, A. (2008). Visualizing
888 glutamatergic cell bodies and synapses inDrosophila larval and adult CNS. *The*
889 *Journal of Comparative Neurology*, *508*, 131–152.
890 https://doi.org/10.1002/cne.21670
891 Dillon, S. C., Zhang, X., Trievel, R. C., & Cheng, X. (2005). The SET-domain protein
892 superfamily: protein lysine methyltransferases. *Genome Biology*, *6*, 227.
893 https://doi.org/10.1186/gb-2005-6-8-227
894 Dorogova, N. V, Fedorova, E. V, Bolobolova, E. U., Ogienko, A. A., & Baricheva, E.

895 M. (2014). GAGA protein is essential for male germ cell development
896 inDrosophila. *Genesis*, *52*, 738–751. https://doi.org/10.1002/dvg.22789
897 Ebihara, T., Guo, F., Zhang, L., Kim, J. Y., & Saffen, D. (2006). Muscarinic
898 Acetylcholine Receptors Stimulate Ca2+ Influx in PC12D Cells Predominantly
899 via Activation of Ca2+ Store–Operated Channels. *The Journal of Biochemistry*,
900 *139*, 449–458. https://doi.org/10.1093/jb/mvj064
901 Finogenova, K., Bonnet, J., Poepsel, S., Schäfer, I. B., Finkl, K., Schmid, K., Litz, C.,
902 Strauss, M., Benda, C., & Müller, J. (2020). Structural basis for PRC2 decoding
903 of active histone methylation marks H3K36me2/3. *ELife*, *9*.
904 https://doi.org/10.7554/elife.61964
905 Gaskill, M. M., Gibson, T. J., Larson, E. D., & Harrison, M. M. (2021). GAF is
906 essential for zygotic genome activation and chromatin accessibility in the early
907 Drosophila embryo. *ELife*, *10*. https://doi.org/10.7554/elife.66668
908 Geng, H., Chen, H., Wang, H., & Wang, L. (2021). The Histone Modifications of
909 Neuronal Plasticity. *Neural Plasticity*, *2021*, 1–7.
910 https://doi.org/10.1155/2021/6690523
911 Gilbert, L. A., Larson, M. H., Morsut, L., Liu, Z., Brar, G. A., Torres, S. E., Stern-
912 Ginossar, N., Brandman, O., Whitehead, E. H., Doudna, J. A., Lim, W. A.,
913 Weissman, J. S., & Qi, L. S. (2013). CRISPR-Mediated Modular RNA-Guided
914 Regulation of Transcription in Eukaryotes. *Cell*, *154*, 442–451.
915 https://doi.org/10.1016/j.cell.2013.06.044
916 Goedhart, J. (2020). PlotTwist: A web app for plotting and annotating continuous
917 data. *PLOS Biology*, *18*, e3000581. https://doi.org/10.1371/journal.pbio.3000581
918 Goedhart, J. (2021). SuperPlotsOfData—a web app for the transparent display and
919 quantitative comparison of continuous data from different conditions. *Molecular
920 Biology of the Cell*, *32*, 470–474. https://doi.org/10.1091/mbc.e20-09-0583
921 Govorunova, E. G., Sineshchekov, O. A., Janz, R., Liu, X., & Spudich, J. L. (2015).
922 Natural light-gated anion channels: A family of microbial rhodopsins for
923 advanced optogenetics. *Science*, *349*, 647–650.
924 https://doi.org/10.1126/science.aaa7484
925 Greenberg, A. J., Yanowitz, J. L., & Schedl, P. (2004). The Drosophila GAGA Factor
926 Is Required for Dosage Compensation in Males and for the Formation of the

927 Male-Specific-Lethal Complex Chromatin Entry Site at 12DE. *Genetics*, *166*,
928 279–289. https://doi.org/10.1534/genetics.166.1.279
929 Gu, X., & Spitzer, N. C. (1995). Distinct aspects of neuronal differentiation encoded
930 by frequency of spontaneous Ca2+ transients. *Nature*, *375*, 784–787.
931 https://doi.org/10.1038/375784a0
932 Hardie, R. C., Peretz, A., Suss-Toby, E., Rom-Glas, A., Bishop, S. A., Selinger, Z., &
933 Minke, B. (1993). Protein kinase C is required for light adaptation in Drosophila
934 photoreceptors. *Nature*, *363*, 634–637. https://doi.org/10.1038/363634a0
935 Hasan, G., & Sharma, A. (2020). Regulation of neuronal physiology by Ca2+ release
936 through the IP3R. *Current Opinion in Physiology*, *17*, 1–8.
937 https://doi.org/10.1016/j.cophys.2020.06.001
938 Ho, J., Tumkaya, T., Aryal, S., Choi, H., & Claridge-Chang, A. (2018). Moving
939 beyond *P* values: Everyday data analysis with estimation plots. *BioArxiv*.
940 https://doi.org/10.1101/377978
941 Hogan, P. G., Chen, L., Nardone, J., & Rao, A. (2003). Transcriptional regulation by
942 calcium, calcineurin, and NFAT. *Genes & Development*, *17*, 2205–2232.
943 https://doi.org/10.1101/gad.1102703
944 Hu, Y., Comjean, A., Perrimon, N., & Mohr, S. E. (2017). The Drosophila Gene
945 Expression Tool (DGET) for expression analyses. *BMC Bioinformatics*, *18*(1), 1–
946 9. https://doi.org/10.1186/s12859-017-1509-z
947 Huang, D. W., Sherman, B. T., & Lempicki, R. A. (2008). Systematic and integrative
948 analysis of large gene lists using DAVID bioinformatics resources. *Nature*
949 *Protocols*, *4*, 44–57. https://doi.org/10.1038/nprot.2008.211
950 Huang, D. W., Sherman, B. T., & Lempicki, R. A. (2009). Systematic and integrative
951 analysis of large gene lists using DAVID bioinformatics resources. *Nature*
952 *Protocols*, *4*(1), 44–57. https://doi.org/10.1038/nprot.2008.211
953 Jarvilehto, M., & Finell, N. (1983). Development of the function of visual receptor
954 cells during the pupal life of the flyCalliphora. *Journal of Comparative*
955 *Physiology ? A*, *150*, 529–536. https://doi.org/10.1007/bf00609579
956 Johns, D. C., Marx, R., Mains, R. E., O'Rourke, B., & Marbán, E. (1999). Inducible
957 Genetic Suppression of Neuronal Excitability. *The Journal of Neuroscience*, *19*,
958 1691–1697. https://doi.org/10.1523/jneurosci.19-05-01691.1999

959 Johnson-Venkatesh, E. M., Khan, M. N., Murphy, G. G., Sutton, M. A., & Umemori,
960 H. (2015). Excitability governs neural development in a hippocampal region
961 specific manner. *Development*. https://doi.org/10.1242/dev.121202
962 Joshi, R., Venkatesh, K., Srinivas, R., Nair, S., & Hasan, G. (2004). Genetic
963 Dissection of itpr Gene Function Reveals a Vital Requirement in Aminergic Cells
964 of Drosophila Larvae. *Genetics*, *166*(1), 225–236.
965 https://doi.org/10.1534/genetics.166.1.225
966 Kaeser, P. S., & Regehr, W. G. (2017). The readily releasable pool of synaptic
967 vesicles. *Current Opinion in Neurobiology*, *43*, 63–70.
968 https://doi.org/10.1016/j.conb.2016.12.012
969 Keyser, P., Borge-Renberg, K., & Hultmark, D. (2007). The Drosophila NFAT
970 homolog is involved in salt stress tolerance. *Insect Biochemistry and Molecular*
971 *Biology*, *37*, 356–362. https://doi.org/10.1016/j.ibmb.2006.12.009
972 Kim, D., Langmead, B., & Salzberg, S. L. (2015). HISAT: A fast spliced aligner with
973 low memory requirements. *Nature Methods*, *12*(4), 357–360.
974 https://doi.org/10.1038/nmeth.3317
975 Kim, D., Paggi, J. M., Park, C., Bennett, C., & Salzberg, S. L. (2019). Graph-based
976 genome alignment and genotyping with HISAT2 and HISAT-genotype. *Nature*
977 *Biotechnology*, *37*(8), 907–915. https://doi.org/10.1038/s41587-019-0201-4
978 Kishi, Y., & Gotoh, Y. (2018). Regulation of Chromatin Structure During Neural
979 Development. *Frontiers in Neuroscience*, *12*.
980 https://doi.org/10.3389/fnins.2018.00874
981 Kitamoto, T. (2001). Conditional modification of behavior inDrosophila by targeted
982 expression of a temperature-sensitiveshibire allele in defined neurons. *Journal*
983 *of Neurobiology*, *47*, 81–92. https://doi.org/10.1002/neu.1018
984 Klapoetke, N. C., Murata, Y., Kim, S. S., Pulver, S. R., Birdsey-Benson, A., Cho, Y.
985 K., Morimoto, T. K., Chuong, A. S., Carpenter, E. J., Tian, Z., Wang, J., Xie, Y.,
986 Yan, Z., Zhang, Y., Chow, B. Y., Surek, B., Melkonian, M., Jayaraman, V.,
987 Constantine-Paton, M., … Boyden, E. S. (2014). Independent optical excitation
988 of distinct neural populations. *Nature Methods*, *11*, 338–346.
989 https://doi.org/10.1038/nmeth.2836
990 Kong, E. C., Woo, K., Li, H., Lebestky, T., Mayer, N., Sniffen, M. R., Heberlein, U.,

991 Bainton, R. J., Hirsh, J., & Wolf, F. W. (2010). A Pair of Dopamine Neurons
992 Target the D1-Like Dopamine Receptor DopR in the Central Complex to
993 Promote Ethanol-Stimulated Locomotion in Drosophila. *PLoS ONE*, *5*.
994 https://doi.org/10.1371/journal.pone.0009954
995 Krogan, N. J., Kim, M., Tong, A., Golshani, A., Cagney, G., Canadien, V., Richards,
996 D. P., Beattie, B. K., Emili, A., Boone, C., Shilatifard, A., Buratowski, S., &
997 Greenblatt, J. (2003). Methylation of Histone H3 by Set2 in *Saccharomyces*
998 *cerevisiae* Is Linked to Transcriptional Elongation by RNA Polymerase II.
999 *Molecular and Cellular Biology*, *23*, 4207–4218.
1000 https://doi.org/10.1128/mcb.23.12.4207-4218.2003
1001 Larkin, A., Marygold, S. J., Antonazzo, G., Attrill, H., dos Santos, G., Garapati, P. V,
1002 Goodman, J. L., Gramates, L. S., Millburn, G., Strelets, V. B., Tabone, C. J.,
1003 Thurmond, J., Perrimon, N., Gelbart, S. R., Agapite, J., Broll, K., Crosby, M., dos
1004 Santos, G., Falls, K., … Lovato, T. (2020). FlyBase: updates to the Drosophila
1005 melanogaster knowledge base. *Nucleic Acids Research*, *49*, D899–D907.
1006 https://doi.org/10.1093/nar/gkaa1026
1007 Leinwand, S. G., & Scott, K. (2021). Juvenile hormone drives the maturation of
1008 spontaneous mushroom body neural activity and learned behavior. *Neuron*, *109*,
1009 1836-1847.e5. https://doi.org/10.1016/j.neuron.2021.04.006
1010 Levine, R. B. (1984). Changes in Neuronal Circuits During Insect Metamorphosis.
1011 *Journal of Experimental Biology*, *112*, 27–44.
1012 https://doi.org/10.1242/jeb.112.1.27
1013 Li, J., Liu, Y., Rhee, H. S., Ghosh, S. K. B., Bai, L., Pugh, B. F., & Gilmour, D. S.
1014 (2013). Kinetic Competition between Elongation Rate and Binding of NELF
1015 Controls Promoter-Proximal Pausing. *Molecular Cell*, *50*(5), 711–722.
1016 https://doi.org/10.1016/j.molcel.2013.05.016
1017 Liao, Y., Smyth, G. K., & Shi, W. (2014). FeatureCounts: An efficient general
1018 purpose program for assigning sequence reads to genomic features.
1019 *Bioinformatics*, *30*(7), 923–930. https://doi.org/10.1093/bioinformatics/btt656
1020 Lichtinghagen, R., Stocker, M., Wittka, R., Boheim, G., Stühmer, W., Ferrus, A., &
1021 Pongs, O. (1990). Molecular basis of altered excitability in Shaker mutants of
1022 Drosophila melanogaster. *The EMBO Journal*, *9*, 4399–4407.

https://doi.org/10.1002/j.1460-2075.1990.tb07890.x

Lieberman, O. J., McGuirt, A. F., Mosharov, E. V, Pigulevskiy, I., Hobson, B. D., Choi, S., Frier, M. D., Santini, E., Borgkvist, A., & Sulzer, D. (2018). Dopamine Triggers the Maturation of Striatal Spiny Projection Neuron Excitability during a Critical Period. *Neuron*, *99*, 540-554.e4. https://doi.org/10.1016/j.neuron.2018.06.044

Liu, C., Plaçais, P.-Y., Yamagata, N., Pfeiffer, B. D., Aso, Y., Friedrich, A. B., Siwanowicz, I., Rubin, G. M., Preat, T., & Tanimoto, H. (2012). A subset of dopamine neurons signals reward for odour memory in Drosophila. *Nature*, *488*, 512–516. https://doi.org/10.1038/nature11304

Lomaev, D., Mikhailova, A., Erokhin, M., Shaposhnikov, A. V, Moresco, J. J., Blokhina, T., Wolle, D., Aoki, T., Ryabykh, V., Yates, J. R., Shidlovskii, Y. V, Georgiev, P., Schedl, P., & Chetverina, D. (2017). The GAGA factor regulatory network: Identification of GAGA factor associated proteins. *PLOS ONE*, *12*, e0173602. https://doi.org/10.1371/journal.pone.0173602

Love, M. I., Huber, W., & Anders, S. (2014). Moderated estimation of fold change and dispersion for RNA-seq data with DESeq2. *Genome Biology*, *15*(12), 1–21. https://doi.org/10.1186/s13059-014-0550-8

Mahmoudi, T. (2003). GAGA facilitates binding of Pleiohomeotic to a chromatinized Polycomb response element. *Nucleic Acids Research*, *31*(14), 4147–4156. https://doi.org/10.1093/nar/gkg479

Manjila, S., & Hasan, G. (2018). Flight and Climbing Assay for Assessing Motor Functions in Drosophila. *BIO-PROTOCOL*, *8*. https://doi.org/10.21769/bioprotoc.2742

Mao, Z., & Davis, R. (2009). Eight different types of dopaminergic neurons innervate the Drosophila mushroom body neuropil: anatomical and physiological heterogeneity. *Frontiers in Neural Circuits*, *3*. https://doi.org/10.3389/neuro.04.005.2009

Marder, E. (2012). Neuromodulation of Neuronal Circuits: Back to the Future. *Neuron*, *76*, 1–11. https://doi.org/10.1016/j.neuron.2012.09.010

Margueron, R., & Reinberg, D. (2011). The Polycomb complex PRC2 and its mark in life. *Nature*, *469*, 343–349. https://doi.org/10.1038/nature09784

1055 Mayseless, O., Shapira, G., Rachad, E. Y., Fiala, A., & Schuldiner, O. (2023).
1056 Neuronal excitability as a regulator of circuit remodeling. *Current Biology*, *33*,
1057 981-989.e3. https://doi.org/10.1016/j.cub.2023.01.032
1058 McGuire, S. E., Mao, Z., & Davis, R. L. (2004). Spatiotemporal Gene Expression
1059 Targeting with the TARGET and Gene-Switch Systems in Drosophila. *Science*
1060 *Signaling*, *2004*, pl6–pl6. https://doi.org/10.1126/stke.2202004pl6
1061 McKinney, A., Petrova, R., & Panagiotakos, G. (2022). Calcium and activity-
1062 dependent signaling in the developing cerebral cortex. *Development*, *149*.
1063 https://doi.org/10.1242/dev.198853
1064 Megha, & Hasan, G. (2017). IP3R-mediated Ca2+ release regulates protein
1065 metabolism in drosophila neuroendocrine cells: Implications for development
1066 under nutrient stress. *Development (Cambridge)*, *144*(8), 1484–1489.
1067 https://doi.org/10.1242/dev.145235
1068 Metsalu, T., & Vilo, J. (2015). ClustVis: A web tool for visualizing clustering of
1069 multivariate data using Principal Component Analysis and heatmap. *Nucleic*
1070 *Acids Research*, *43*(W1), W566–W570. https://doi.org/10.1093/nar/gkv468
1071 Mitra, R., & Hasan, G. (2022). Store-operated Ca2+ entry regulates neuronal gene
1072 expression and function. *Current Opinion in Neurobiology*, *73*, 102520.
1073 https://doi.org/10.1016/j.conb.2022.01.005
1074 Mitra, R., Richhariya, S., Jayakumar, S., Notani, D., & Hasan, G. (2020). IP3/Ca2+
1075 signals regulate larval to pupal transition under nutrient stress through the
1076 H3K36 methyltransferase dSET2. *BioRxiv*.
1077 https://doi.org/10.1101/2020.11.25.399329
1078 modENCODE Consortium, Roy, S., Ernst, J., Kharchenko, P. V, Kheradpour, P.,
1079 Negre, N., Eaton, M. L., Landolin, J. M., Bristow, C. A., Ma, L., Lin, M. F.,
1080 Washietl, S., Arshinoff, B. I., Ay, F., Meyer, P. E., Robine, N., Washington, N. L.,
1081 Di Stefano, L., Berezikov, E., … Kellis, M. (2010). Identification of functional
1082 elements and regulatory circuits by Drosophila modENCODE. *Science (New*
1083 *York, N.Y.)*, *330*, 1787–1797. https://doi.org/10.1126/science.1198374
1084 Nitabach, M. N. (2006). Electrical Hyperexcitation of Lateral Ventral Pacemaker
1085 Neurons Desynchronizes Downstream Circadian Oscillators in the Fly Circadian
1086 Circuit and Induces Multiple Behavioral Periods. *Journal of Neuroscience*, *26*,

479–489. https://doi.org/10.1523/jneurosci.3915-05.2006

O'Hare, J. K., Gonzalez, K. C., Herrlinger, S. A., Hirabayashi, Y., Hewitt, V. L., Blockus, H., Szoboszlay, M., Rolotti, S. V, Geiller, T. C., Negrean, A., Chelur, V., Polleux, F., & Losonczy, A. (2022). Compartment-specific tuning of dendritic feature selectivity by intracellular Ca2+ release. *Science*, *375*. https://doi.org/10.1126/science.abm1670

Owald, D., Felsenberg, J., Talbot, C. B., Das, G., Perisse, E., Huetteroth, W., & Waddell, S. (2015). Activity of Defined Mushroom Body Output Neurons Underlies Learned Olfactory Behavior in Drosophila. *Neuron*, *86*, 417–427. https://doi.org/10.1016/j.neuron.2015.03.025

Pathak, T., Agrawal, T., Richhariya, S., Sadaf, S., & Hasan, G. (2015). Store-Operated Calcium Entry through Orai Is Required for Transcriptional Maturation of the Flight Circuit in *Drosophila*. *The Journal of Neuroscience*, *35*, 13784–13799. https://doi.org/10.1523/jneurosci.1680-15.2015

Ping, Y., Waro, G., Licursi, A., Smith, S., Vo-Ba, D.-A., & Tsunoda, S. (2011). Shal/Kv4 Channels Are Required for Maintaining Excitability during Repetitive Firing and Normal Locomotion in Drosophila. *PLoS ONE*, *6*, e16043. https://doi.org/10.1371/journal.pone.0016043

Postma, M., & Goedhart, J. (2019). PlotsOfData—A web app for visualizing data together with their summaries. *PLOS Biology*, *17*, e3000202. https://doi.org/10.1371/journal.pbio.3000202

Prakriya, M., & Lewis, R. S. (2015). STORE-OPERATED CALCIUM CHANNELS. *Physiol Rev*, *307*, 1383–1436. https://doi.org/10.1152/physrev.00020.2014

Ramírez, F., Ryan, D. P., Grüning, B., Bhardwaj, V., Kilpert, F., Richter, A. S., Heyne, S., Dündar, F., & Manke, T. (2016). deepTools2: a next generation web server for deep-sequencing data analysis. *Nucleic Acids Research*, *44*(W1), W160–W165. https://doi.org/10.1093/nar/gkw257

Richhariya, S., Jayakumar, S., Abruzzi, K., Rosbash, M., & Hasan, G. (2017). A pupal transcriptomic screen identifies Ral as a target of store-operated calcium entry in Drosophila neurons. *Scientific Reports*, *7*(1), 1–12. https://doi.org/10.1038/srep42586

Riemensperger, T., Völler, T., Stock, P., Buchner, E., & Fiala, A. (2005). Punishment

1119 Prediction by Dopaminergic Neurons in Drosophila. *Current Biology*, *15*, 1953–
1120 1960. https://doi.org/10.1016/j.cub.2005.09.042
1121 Ritchie, M. E., Phipson, B., Wu, D., Hu, Y., Law, C. W., Shi, W., & Smyth, G. K.
1122 (2015). limma powers differential expression analyses for RNA-sequencing and
1123 microarray studies. *Nucleic Acids Research*, *43*, e47–e47.
1124 https://doi.org/10.1093/nar/gkv007
1125 Robinson, M. D., McCarthy, D. J., & Smyth, G. K. (2009). edgeR: A Bioconductor
1126 package for differential expression analysis of digital gene expression data.
1127 *Bioinformatics*, *26*(1), 139–140. https://doi.org/10.1093/bioinformatics/btp616
1128 Rosenberg, S. S., & Spitzer, N. C. (2011). Calcium Signaling in Neuronal
1129 Development. *Cold Spring Harbor Perspectives in Biology*, *3*, a004259–
1130 a004259. https://doi.org/10.1101/cshperspect.a004259
1131 Schindelin, J., Arganda-Carreras, I., Frise, E., Kaynig, V., Longair, M., Pietzsch, T.,
1132 Preibisch, S., Rueden, C., Saalfeld, S., Schmid, B., Tinevez, J. Y., White, D. J.,
1133 Hartenstein, V., Eliceiri, K., Tomancak, P., & Cardona, A. (2012). Fiji: An open-
1134 source platform for biological-image analysis. *Nature Methods*, *9*(7), 676–682.
1135 https://doi.org/10.1038/nmeth.2019
1136 Shakiryanova, D., Morimoto, T., Zhou, C., Chouhan, A. K., Sigrist, S. J., Nose, A.,
1137 Macleod, G. T., Deitcher, D. L., & Levitan, E. S. (2011). Differential Control of
1138 Presynaptic CaMKII Activation and Translocation to Active Zones. *Journal of*
1139 *Neuroscience*, *31*, 9093–9100. https://doi.org/10.1523/jneurosci.0550-11.2011
1140 Sharma, A., & Hasan, G. (2020). Modulation of flight and feeding behaviours
1141 requires presynaptic IP3Rs in dopaminergic neurons. *ELife*, *9*.
1142 https://doi.org/10.7554/elife.62297
1143 Shimojima, T. (2003). Drosophila FACT contributes to Hox gene expression through
1144 physical and functional interactions with GAGA factor. *Genes & Development*,
1145 *17*(13), 1605–1616. https://doi.org/10.1101/gad.1086803
1146 Singh, S., & Wu, C. F. (1990). Properties of potassium currents and their role in
1147 membrane excitability in Drosophila larval muscle fibers. *Journal of*
1148 *Experimental Biology*, *152*, 59–76. https://doi.org/10.1242/jeb.152.1.59
1149 Somasundaram, A., Shum, A. K., McBride, H. J., Kessler, J. A., Feske, S., Miller, R.
1150 J., & Prakriya, M. (2014). Store-Operated CRAC Channels Regulate Gene

1151 Expression and Proliferation in Neural Progenitor Cells. *Journal of*
1152 *Neuroscience*, *34*, 9107–9123. https://doi.org/10.1523/jneurosci.0263-14.2014
1153 Spitzer, N. C. (2012). Activity-dependent neurotransmitter respecification. *Nature*
1154 *Reviews Neuroscience*, *13*, 94–106. https://doi.org/10.1038/nrn3154
1155 Stabell, M., Larsson, J., Aalen, R. B., & Lambertsson, A. (2007). Drosophila dSet2
1156 functions in H3-K36 methylation and is required for development. *Biochemical*
1157 *and Biophysical Research Communications*, *359*, 784–789.
1158 https://doi.org/10.1016/j.bbrc.2007.05.189
1159 Streb, H., Bayerdörffer, E., Haase, W., Irvine, R. F., & Schulz, I. (1984). Effect of
1160 inositol-1,4,5-trisphosphate on isolated subcellular fractions of rat pancreas. *The*
1161 *Journal of Membrane Biology*, *81*, 241–253. https://doi.org/10.1007/bf01868717
1162 Sugie, A., Marchetti, G., & Tavosanis, G. (2018). Structural aspects of plasticity in
1163 the nervous system of Drosophila. *Neural Development*, *13*.
1164 https://doi.org/10.1186/s13064-018-0111-z
1165 Sun, F., Zeng, J., Jing, M., Zhou, J., Feng, J., Owen, S. F., Luo, Y., Li, F., Wang, H.,
1166 Yamaguchi, T., Yong, Z., Gao, Y., Peng, W., Wang, L., Zhang, S., Du, J., Lin,
1167 D., Xu, M., Kreitzer, A. C., … Li, Y. (2018). A Genetically Encoded Fluorescent
1168 Sensor Enables Rapid and Specific Detection of Dopamine in Flies, Fish, and
1169 Mice. *Cell*, *174*, 481-496.e19. https://doi.org/10.1016/j.cell.2018.06.042
1170 Sweeney, S. T., Broadie, K., Keane, J., Niemann, H., & O'Kane, C. J. (1995).
1171 Targeted expression of tetanus toxin light chain in Drosophila specifically
1172 eliminates synaptic transmission and causes behavioral defects. *Neuron*, *14*,
1173 341–351. https://doi.org/10.1016/0896-6273(95)90290-2
1174 Taber, K. H., & Hurley, R. A. (2014). Volume Transmission in the Brain: Beyond the
1175 Synapse. *The Journal of Neuropsychiatry and Clinical Neurosciences*, *26*, iv–4.
1176 https://doi.org/10.1176/appi.neuropsych.13110351
1177 Takechi, H., Eilers, J., & Konnerth, A. (1998). A new class of synaptic response
1178 involving calcium release in dendritic spines. *Nature*, *396*, 757–760.
1179 https://doi.org/10.1038/25547
1180 Tang, X., Li, T., Liu, S., Wisniewski, J., Zheng, Q., Rong, Y., Lavis, L. D., & Wu, C.
1181 (2022). Kinetic principles underlying pioneer function of GAGA transcription
1182 factor in live cells. *Nature Structural & Molecular Biology*, *29*, 665–676.

1183 https://doi.org/10.1038/s41594-022-00800-z
1184 Thillaiappan, N. B., Chakraborty, P., Hasan, G., & Taylor, C. W. (2019). IP3
1185 receptors and Ca2+ entry. *Biochimica et Biophysica Acta (BBA) - Molecular Cell*
1186 *Research*, *1866*, 1092–1100. https://doi.org/10.1016/j.bbamcr.2018.11.007
1187 Truszkowski, T. L. S., & Aizenman, C. D. (2015). Neurobiology: Setting the Set Point
1188 for Neural Homeostasis. *Current Biology*, *25*, R1132–R1133.
1189 https://doi.org/10.1016/j.cub.2015.10.021
1190 Tsai, S.-Y., Chang, Y.-L., Swamy, K. B. S., Chiang, R.-L., & Huang, D.-H. (2016).
1191 GAGA factor, a positive regulator of global gene expression, modulates
1192 transcriptional pausing and organization of upstream nucleosomes. *Epigenetics*
1193 *& Chromatin*, *9*. https://doi.org/10.1186/s13072-016-0082-4
1194 Tsao, C.-H., Chen, C.-C., Lin, C.-H., Yang, H.-Y., & Lin, S. (2018). Drosophila
1195 mushroom bodies integrate hunger and satiety signals to control innate food-
1196 seeking behavior. *ELife*, *7*. https://doi.org/10.7554/elife.35264
1197 Tsukiyama, T., Becker, P. B., & Wu, C. (1994). ATP-dependent nucleosome
1198 disruption at a heat-shock promoter mediated by binding of GAGA transcription
1199 factor. *Nature*, *367*(6463), 525–532. https://doi.org/10.1038/367525a0
1200 Venkiteswaran, G., & Hasan, G. (2009). Intracellular Ca2+ signalling and store
1201 operated Ca2+ entry are required in Drosophila neurons for flight. *Proceedings*
1202 *of the National Academy of Sciences*, *2009*.
1203 Verma, S. K., Tian, X., LaFrance, L. V, Duquenne, C., Suarez, D. P., Newlander, K.
1204 A., Romeril, S. P., Burgess, J. L., Grant, S. W., Brackley, J. A., Graves, A. P.,
1205 Scherzer, D. A., Shu, A., Thompson, C., Ott, H. M., Aller, G. S. Van, Machutta,
1206 C. A., Diaz, E., Jiang, Y., … Miller, W. H. (2012). Identification of Potent,
1207 Selective, Cell-Active Inhibitors of the Histone Lysine Methyltransferase EZH2.
1208 *ACS Medicinal Chemistry Letters*, *3*, 1091–1096.
1209 https://doi.org/10.1021/ml3003346
1210 Viswanath, V., Story, G. M., Peier, A. M., Petrus, M. J., Lee, V. M., Hwang, S. W.,
1211 Patapoutian, A., & Jegla, T. (2003). Opposite thermosensor in fruitfly and
1212 mouse. *Nature*, *423*, 822–823. https://doi.org/10.1038/423822a
1213 Waddell, S. (2016). Neural Plasticity: Dopamine Tunes the Mushroom Body Output
1214 Network. *Current Biology*, *26*, R109–R112.

https://doi.org/10.1016/j.cub.2015.12.023

Wang, Y., Deng, X., & Gill, D. L. (2010). Calcium Signaling by STIM and Orai: Intimate Coupling Details Revealed. *Science Signaling*, *3*, pe42–pe42. https://doi.org/10.1126/scisignal.3148pe42

Weiss, S., Melom, J. E., Ormerod, K. G., Zhang, Y. V, & Littleton, J. T. (2019). Glial Ca2+signaling links endocytosis to K+ buffering around neuronal somas to regulate excitability. *ELife*, *8*. https://doi.org/10.7554/elife.44186

Wilkins, R. C., & Lis, J. T. (1999). DNA distortion and multimerization: novel functions of the glutamine-rich domain of GAGA factor 1 1Edited by M. Yaniv. *Journal of Molecular Biology*, *285*(2), 515–525. https://doi.org/10.1006/jmbi.1998.2356

Xu, W., & Lipscombe, D. (2001). Neuronal CaV1.3α1 L-Type Channels Activate at Relatively Hyperpolarized Membrane Potentials and Are Incompletely Inhibited by Dihydropyridines. *The Journal of Neuroscience*, *21*, 5944–5951. https://doi.org/10.1523/JNEUROSCI.21-16-05944.2001

Yagi, R., Mabuchi, Y., Mizunami, M., & Tanaka, N. K. (2016). Convergence of multimodal sensory pathways to the mushroom body calyx in Drosophila melanogaster. *Scientific Reports*, *6*. https://doi.org/10.1038/srep29481

Yeromin, A. V, Zhang, S. L., Jiang, W., Yu, Y., Safrina, O., & Cahalan, M. D. (2006). Molecular identification of the CRAC channel by altered ion selectivity in a mutant of Orai. *Nature*, *443*, 226–229. https://doi.org/10.1038/nature05108

Zambelli, F., Pesole, G., & Pavesi, G. (2009). Pscan: finding over-represented transcription factor binding site motifs in sequences from co-regulated or co-expressed genes. *Nucleic Acids Research*, *37*, W247–W252. https://doi.org/10.1093/nar/gkp464

Zhai, B., Villén, J., Beausoleil, S. A., Mintseris, J., & Gygi, S. P. (2008). Phosphoproteome Analysis of Drosophila melanogaster Embryos. *Journal of Proteome Research*, *7*, 1675–1682. https://doi.org/10.1021/pr700696a

Zolin, A., Cohn, R., Pang, R., Siliciano, A. F., Fairhall, A. L., & Ruta, V. (2021). Context-dependent representations of movement in Drosophila dopaminergic reinforcement pathways. *Nature Neuroscience*, *24*, 1555–1566. https://doi.org/10.1038/s41593-021-00929-y

1247 **Figure 1**

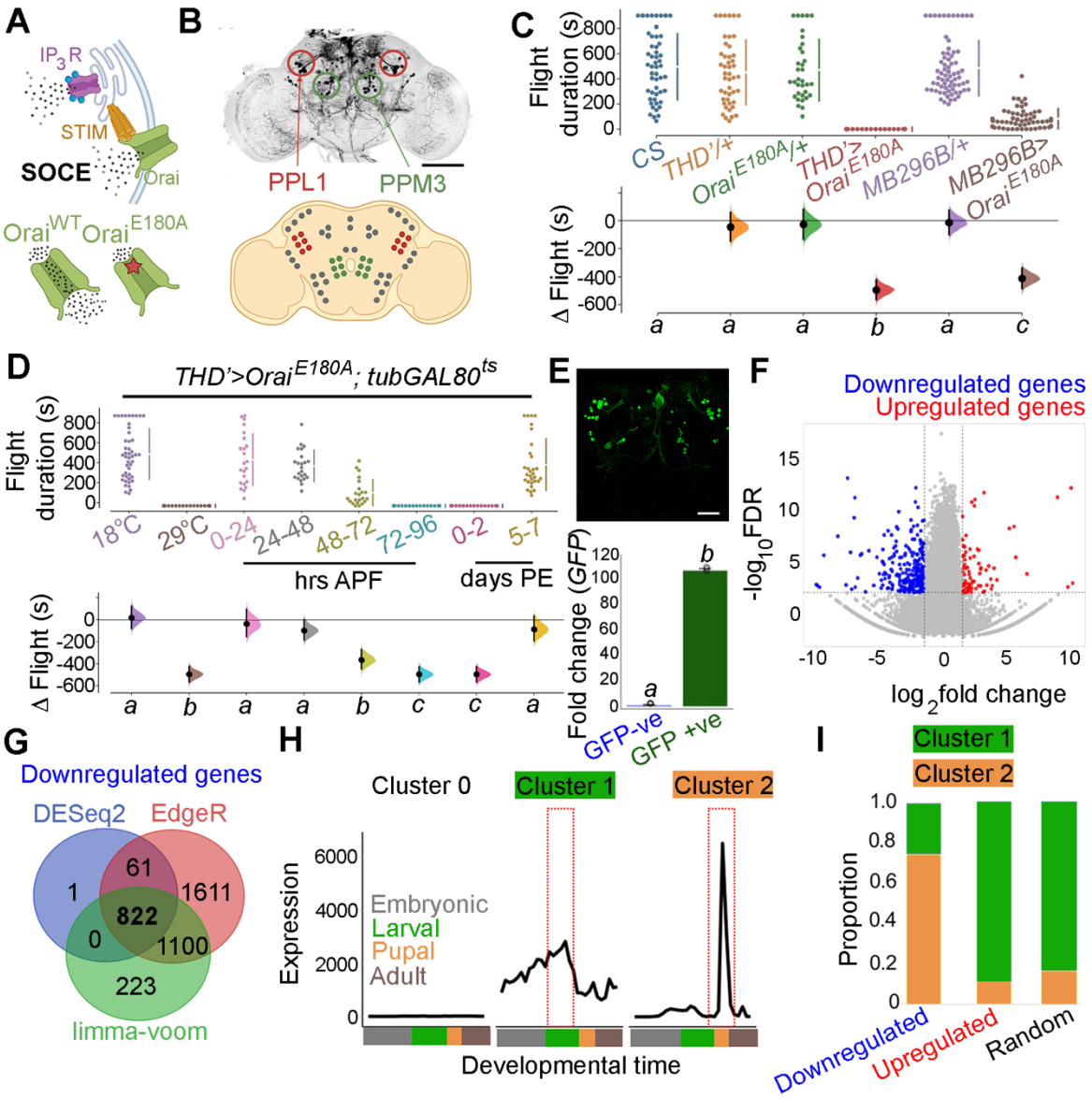

1248 **Figure 1. Orai-mediated Ca^{2+} entry sets the gene expression profile of flight-**
1249 **promoting dopaminergic neurons in late development and early adulthood**.
1250 **A**. A schematic of Ca^{2+} release through the IP_3R and SOCE through STIM/Orai (upper
1251 panel) followed by representation of the wildtype (Ca^{2+} permeable) and mutant (Ca^{2+}
1252 impermeable) Orai channels (lower panel). **B**. Anatomical location of *THD'* DANs in
1253 the fly central brain immunolabelled for mCD8GFP (upper panel) followed by a cartoon
1254 of central brain DAN clusters. Scale bar indicates 20 μm. PPL1 and PPM3 clusters
1255 are labelled in red and green respectively. **C**. Measurement of flight bout durations
1256 demonstrate a requirement for Orai-mediated Ca^{2+} entry in *THD'* DANs and in 2 pairs
1257 of PPL1 DANs marked by the MB296B driver. **D**. *THD'* DANs require Ca^{2+} entry
1258 through Orai at 72-96 hours APF and 0-2 days post eclosion to promote flight. In **C**
1259 and **D** flight bout durations in seconds (s) are represented as a swarm plot where each
1260 genotype is represented by a different color, and each fly as a single data point. The
1261 Δ Flight parameter shown below indicates the mean difference for comparisons
1262 against the shared Canton S control and is shown as a Cumming estimation plot.

Mean differences are plotted as bootstrap sampling distributions. Each 95% confidence interval is indicated by the ends of the vertical error bars. The same letter beneath each distribution refers to statistically indistinguishable groups after performing a Kruskal-Wallis test followed by a post hoc Mann-Whitney U-test ($p<0.005$). At least 30 flies were tested for each genotype. **E**. *THD'* DANs were labelled with cytosolic eGFP (10 μm scale), isolated using FACS and validated for enrichment of *GFP* mRNA by qRT-pCR (lower panel). The qRT-pCR results are from 4 biological replicates with different letters representing statistically distinguishable groups after performing a two-tailed t test ($p<0.05$). **F.** RNA-seq comparison of FAC sorted populations of GFP labelled THD' DANs from *THD'>GFP* and *THD'>GFP;Orai*^{E180A} pupal dissected CNSs. The RNA-Seq data is represented in the form of a volcano plot of fold change vs FDR. Individual dots represent genes, coloured in red (upregulated) or blue (downregulated) by >1 fold. **G.** Downregulated genes were identified by 3 different methods of DEG analysis, quantified and compared as a Venn diagram. **H.** Gene expression trajectories of SOCE-induced DEGs plotted as a function of developmental time (modENCODE Consortium et al., 2010) and clustered into 3 groups using k-means analysis. **I**. The relative proportion of downregulated, upregulated genes, and a random set of genes found in the clusters described in (**H**) indicate that 75% of downregulated genes exhibit a pupal peak of expression.

1291 **Figure 2**

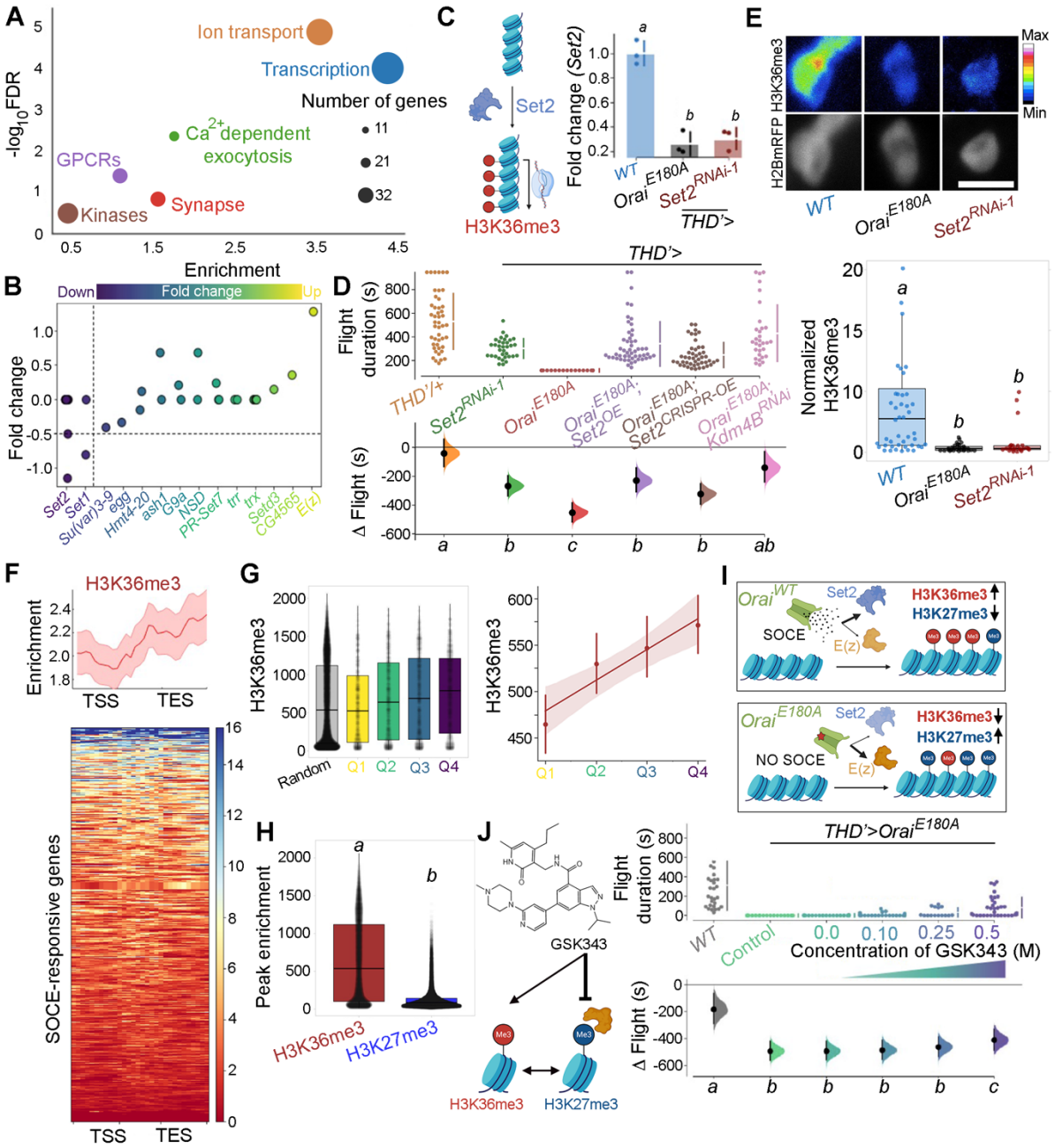

1292 **Figure 2**. **Ca²⁺ entry through Orai regulates gene expression by Set2-mediated**
1293 **histone modification**. **A**. Scatterplot of GO categories enriched in SOCE-responsive
1294 genes. Individual GO terms are represented as differently colored circles, with radius
1295 size indicating number of genes enriched in that category. **B**. Fold change of SET
1296 domain containing genes as indicated. Individual circles on the Y-axis for each gene
1297 represent transcript variants pertaining to that gene. **C**. Transcripts of the H3K36
1298 methyltransferase (left) are significantly diminished (right) in *THD'* DANs either upon
1299 loss of Orai function (*THD'>Orai*^{E180A}) or by knockdown of *Set2* (*THD'>Set2*^{RNAi}). qRT-
1300 PCRs were performed from FAC sorted *THD'* DANs with 3 biological replicates.
1301 Individual $2^{-\Delta\Delta CT}$ values are shown as points. Letters represent statistically
1302 distinguishable groups after performing an ANOVA and post hoc Tukey test ($p<0.05$).
1303 **D**. Significant rescue of flight bout durations seen in *THD' > Orai*^{E180A} flies by

overexpression of *Set2* and by knockdown of the *Kdm4B* demethylase indicating a net requirement for H3K36me3. Flight durations of single flies are depicted as swarm plots and the Δ flight parameter is shown below. Both were measured as described in the legend to Figure 1. N = 30 or more flies for each genotype. Letters represent statistically distinguishable groups after performing an ANOVA and post hoc Tukey test ($p<0.005$) **E**. Representative images (upper panel) and quantification (lower panel) from immunostaining of H3K36me3 and H2BmRFP in nuclei of *THD'* DANs from at least 10 brains. Scale bar represents 5 μm. The boxplot represents individual H3K36me3/H2BmRFP ratios from each *THD'* DAN for each genotype. Letters represent statistically distinguishable groups after performing an ANOVA and post hoc Tukey test ($p<0.05$) **F**. H3K36me3 enrichment over the gene bodies of SOCE-responsive genes in wildtype fly heads represented in the form of a tag density plot. **G**. H3K36me3 signal is enriched on WT SOCE-responsive genes with greater downregulation upon loss of Orai function. Individual data points represent *WT* H3K36me3 ChIP-Seq signals from adult fly heads represented as a boxplot (left) and a regression plot (right; Pearson's correlation coefficient = 0.11) indicating a correlation between extent of downregulation upon loss of SOCE and greater enrichment of H3K36me3. **H**. SOCE-responsive genes are enriched in H3K36me3 signal as compared to H3K27me3 signal as measured from relevant ChIP-Seq datasets. Adult fly head ChIP-Seq datasets for measurements in **F** to **H** were obtained from modEncode (modENCODE Consortium et al., 2010). **I**. Schematic representation of how Orai mediated Ca^{2+} entry regulates a balance of two opposing epigenetic signatures in developing DANs. **J**. Pharmacological inhibition of H3K27me3 using GSKS343 (left) in *THD'>Orai*^{E180A} flies results in a dose-dependent rescue of flight bout durations (right). Flight assay measurements from N> 30 flies, are represented as described earlier. Letters represent statistically distinguishable groups after performing an ANOVA and post hoc Tukey test ($p<0.005$).

1340 **Figure 3**

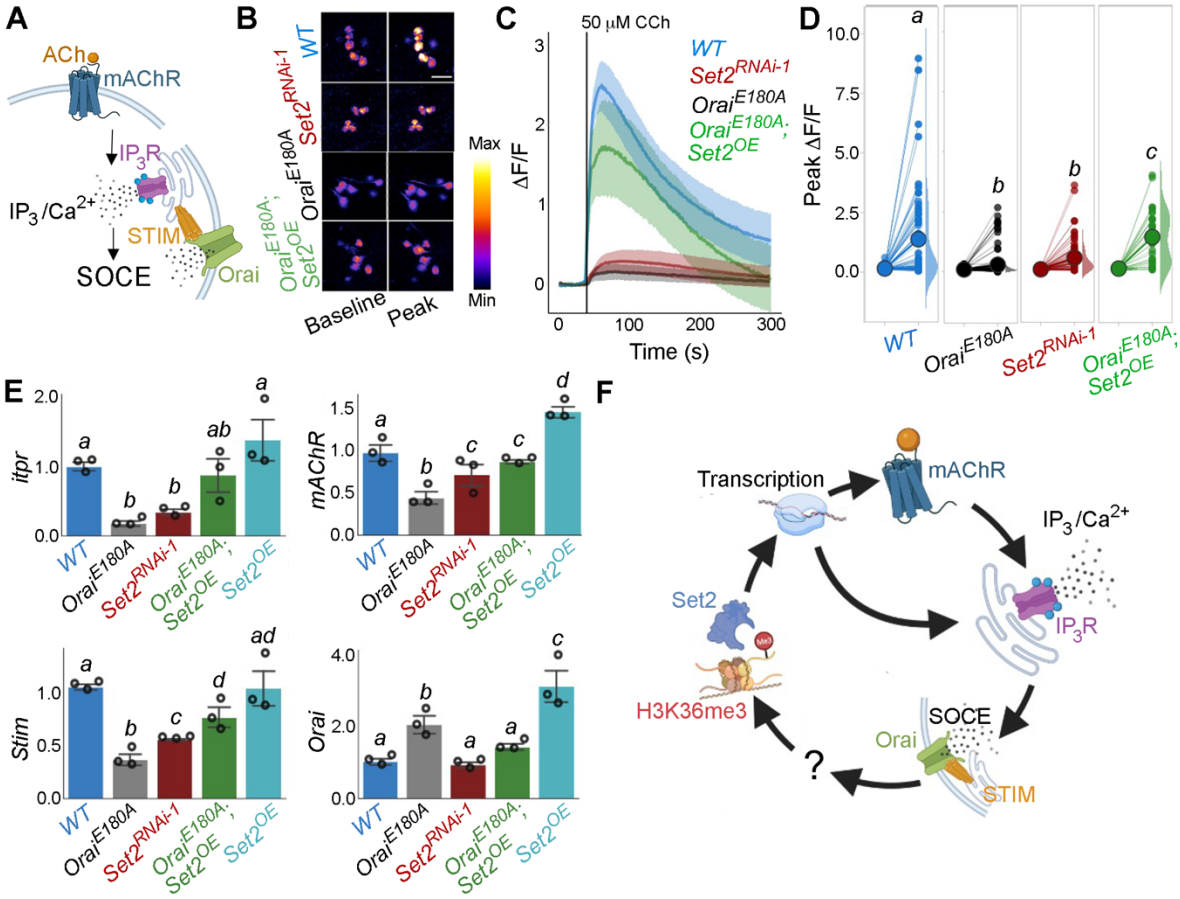

1341 **Figure 3. Orai-mediated Ca^{2+} entry potentiates cellular Ca^{2+} responses to**
1342 **cholinergic inputs through Set2 and a transcriptional feedback loop**
1343 **A**. A schematic of intracellular Ca^{2+} signaling downstream of neuromodulatory
1344 signaling where activation of mAChR stimulates intracellular Ca^{2+} release through the
1345 IP_3R followed by SOCE through STIM/Orai. **B.** Cholinergic inputs by addition of
1346 carbachol (CCh) evoke Ca^{2+} signals as measured by change in the fluorescence of
1347 GCaMP6m in *THD'* DANs of ex-vivo brains. Representative GCaMP6m images of
1348 *THD'* DANs are shown with baseline and peak evoked responses in the indicated
1349 genotypes. Scale bar = 10 μM. **C**. Median GCaMP6m responses plotted as a function
1350 of time. A shaded region around the solid line represents the 95% confidence interval
1351 from 4-5 cells imaged per brain from 10 or more brains per genotype. **D.** Individual
1352 cellular responses depicted as a paired plot where different letters above indicate
1353 statistically distinguishable groups after performing a Kruskal Wallis Test and a Mann-
1354 Whitney U-test ($p<0.05$). **E**. qRT-PCR measurements of *itpr*, *mAChR*, *Stim* and *Orai*
1355 from FAC sorted *THD'* DANs obtained from three biological replicates of appropriate
1356 genetic backgrounds. The genotypes include DANs with loss of cellular Ca^{2+}
1357 responses (*THD'>Orai*^{E180A}; and *THD'>Set2*$^{RNAi-1}$), rescue of cellular Ca^{2+} response by
1358 overexpression of *Set2* (*THD'>Orai*^{E180A}; *Set2*^{OE}) and *Set2* overexpression. Bar plots
1359 indicate mean expression levels in comparison to *rp49*, with individual data points
1360 represented as hollow circles. The letters above indicate statistically indistinguishable
1361 groups after performing a Kruskal Wallis Test and a Mann-Whitney U-test ($p<0.05$). **F**.

Schematic representation of a transcriptional feedback loop downstream of cholinergic stimulation in *THD'* DANs.

Figure 4

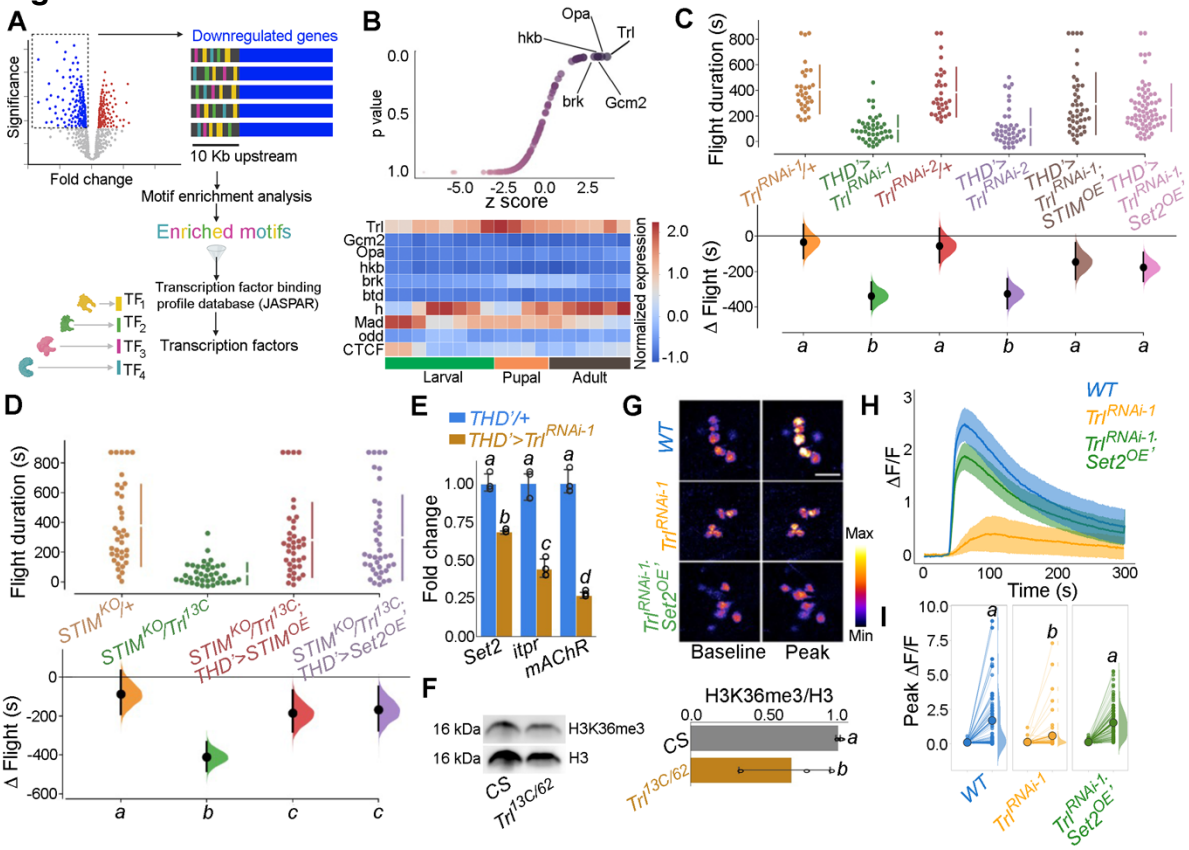

Figure 4. Identification of Trl as an SOCE responsive transcription factor

A. Schematic of motif enrichment analysis for identification of putative SOCE dependent transcription factors (TFs). **B.** Candidate TFs identified (upper panel) and their expression through development (lower panel; modEncode(modENCODE Consortium et al., 2010)) suggests Trl as a top SOCE-responsive candidate TF. **C.** Genetic depletion of *Trl* in *THD'* DANs results in significant flight defects, that can be rescued by overexpression of either *STIM* or *Set2*. **D.** Heteroallelic combination of the *Trl* hypomorphic allele (*Trl*^{13C}) with a *STIM* deficiency causes significant flight deficits, that can be rescued by overexpression of *STIM* or *Set2*. **E.** qRT-PCRs measured relative to *rp49* show reduced *Set2, itpr, and mAChR* levels in *THD'* DANs upon *Trl* knockdown with *Trl*$^{RNAi-1}$. Individual data points of 4 biological replicates are shown as circles and mean expression level as a bar plot (± SEM). The letters above indicate statistically indistinguishable groups after performing a Kruskal Wallis Test and a Mann-Whitney U-test ($p<0.05$). **F**. A representative western blot (left) showing reduced H3K36me3 levels in a *Trl* mutant combination. Quantification of H3K36me3 from 3 biological replicates of *WT* (control) and *Trl* mutant brain lysates (panel on the right). Letters indicate statistically indistinguishable groups after performing a two-tailed t-test ($p<0.05$). **G**. Knockdown of *Trl* in *THD'* neurons attenuate Ca^{2+} response to CCh as shown in representative images of GCamP6m fluorescence quantified in (**H-I**). Scale bar = 10 μM. *Set2* overexpression in the background of *THD'>Trl*^{RNAi} rescues the cholinergic response (**G-I**). Quantification of Ca^{2+} responses are from 10 or more brains per genotype and were performed as described in the legend to Figure 3. The

letters above indicate statistically indistinguishable groups after performing a Kruskal Wallis Test and a Mann-Whitney U-test (p<0.05).

Figure 5

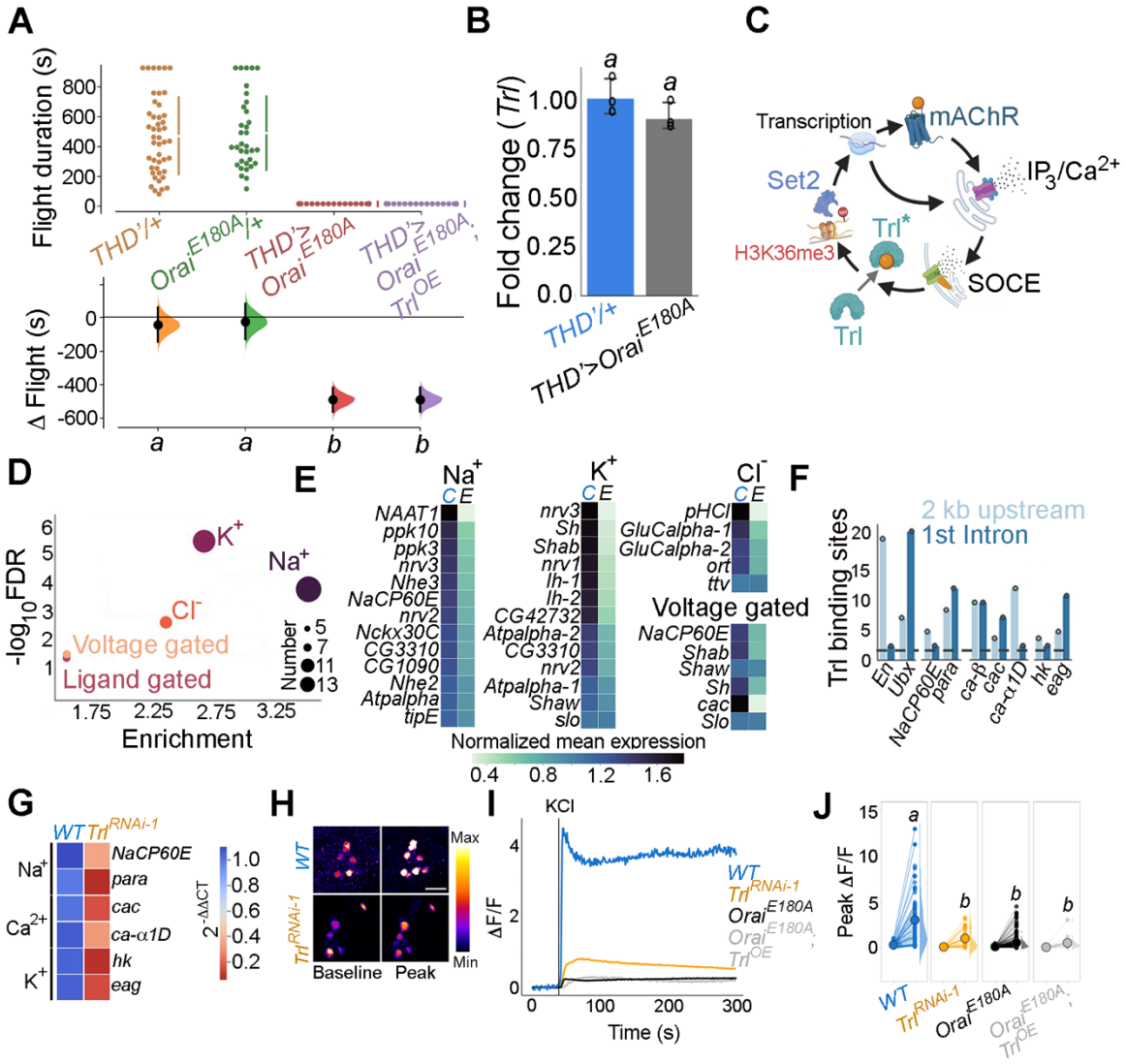

Figure 5. **Trl activity downstream of SOCE is required for *THD'* DAN activity**. A. Overexpression of *WT Trl* is insufficient to rescue flight deficits in *THD'>Orai*^{E180A} flies as evident from flight bout measurements in the indicated genotypes. Flight assay measurements are as described earlier. **B**. *Trl* transcript levels are not altered in *THD'>Orai*^{E180A} neurons with loss of SOCE. qRT-PCR data are measured relative to *rp49*. The bar plot indicates mean expression levels, with individual data points represented as circles. The letters above indicate statistically indistinguishable groups from 3 independent biological replicates after performing a two-tailed t-test (p<0.05). **C**. Schematic with possible Ca^{2+} - mediated activation of Trl downstream of Orai-mediated Ca^{2+} entry (SOCE). **D.** Genes encoding ion channels are enriched among SOCE responsive genes in *THD'* DANs as determined by GO analysis. Circles of varying radii are scaled according to the number of genes enriched in that category. **E**. Downregulation of individual ion channel genes depicted as a heatmap. **F**. Number of Trl binding sites (GAGA repeats) shown as a bar plot in the regulatory regions (2 kb

upstream or 1st intron) of key SOCE-responsive ion channel genes compared to known Trl targets (*En* and *Ubx*). The dashed line indicates the average expected number of Trl targets. **G**. Heatmap of 2^-ΔΔCT values measured using qRT-PCRs from sorted *THD'* DANs with knockdown of *Trl*. **H.** Representative images of KCl-induced depolarizing responses in *THD'* DANs with knockdown of *Trl*. (Scale bar = 10 μM) quantified in **I and J**. Quantification of Ca^{2+} responses are from 10 or more brains per genotype and were performed as described in the legend to Figure 3. The letters above indicate statistically indistinguishable groups after performing a Kruskal Wallis Test and a Mann-Whitney U-test ($p<0.05$).

Figure 6

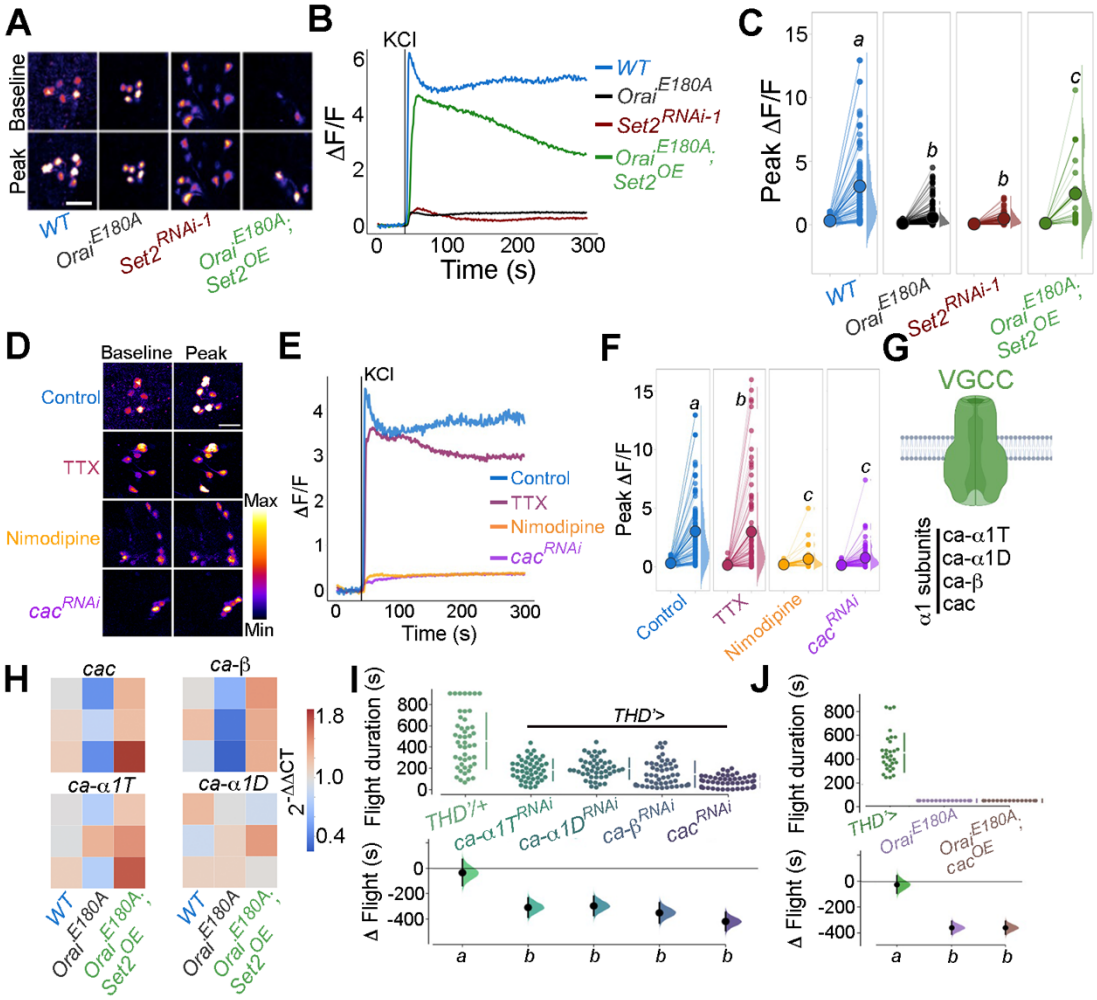

Figure 6. fpDAN excitability requires Orai-mediated Ca^{2+} entry acting through *Set2* -mediated VGCC gene expression. KCl-induced depolarizing responses in *fp*DANs of the indicated genotypes measured using GCaMP6m indicate a requirement for Orai and *Set2*. Representative images **A. (**scale bar = 10 μM), quantified in **B.** and **C**. KCl evoked responses are modulated upon treatment with 10 μM TTX (magenta), 10 μM Nimodipine (orange), and upon cac^{RNAi} (purple)- representative images (scale bar = 10 μM), (**D**), quantified in **E**. Median KCl-evoked GCaMP6m responses plotted as a function of time. The solid line indicates the time point of addition of 70 mM KCl. KCl responses are quantified as a paired plot of peak responses and **F**. with letters

representing statistically indistinguishable groups as measured using a Kruskall Wallis test and post hoc Mann-Whitney U test ($p<0.05$). Quantification of Ca^{2+} responses are from 10 or more brains per genotype and were performed as described in the legend to Figure 3. **G.** Schematic of a typical VGCC and its constituent subunits. **H.** Heatmap of 2^-ΔΔCT values measured using qRT-PCRs from sorted *THD'* DANs show a reduction in the expression of VGCC subunit genes upon loss of Orai function and a rescue by *Set2* overexpression. **I**. Flight assays representing the effect of various VGCC subunit gene RNAis showing flight defects to varying extents. Overexpression of the key VGCC subunit gene-*cac* is required (**I**) but not sufficient (**J**) for restoring flight defects caused by loss of *Orai* function. Flight assay measurements are as described earlier.

Figure 7

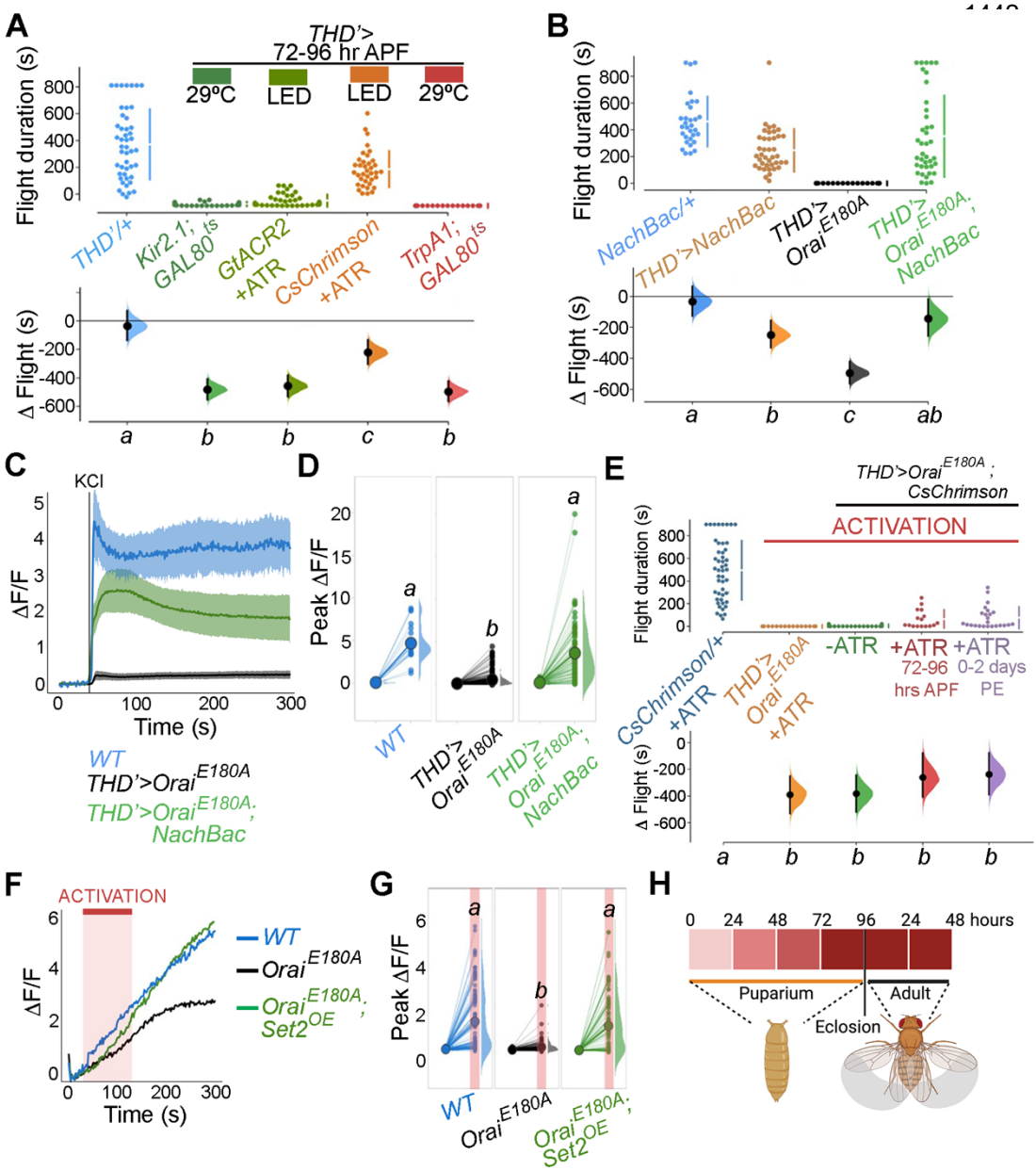

Figure 7. SOCE-mediated gene expression sets the excitability threshold during pupal development **A.** Altering excitability in *THD'* DANs using *Kir2.1* or *GtACR2* mediated inhibition or *CsChrimson* or *TrpA1* during the critical 72-96 hour APF developmental window results in significant flight defects. Orai loss of function phenotypes can be rescued by overexpression of *NachBac* or *CsChrimson* in terms of flight bout durations (**B, E**) and depolarizing KCl responses (**C, D, D, G**). **H.** Schematic for Orai-mediated Ca^{2+} entry regulating expression of key genes that regulate the excitability threshold of dopaminergic neurons regulating flight during a critical developmental window. Flight assays are represented as described earlier, (n>30). Ca^{2+} responses were quantified as described in the legend to Figure 3 and were from 10 or more brains per genotype. Letters above each genotype represent statistically indistinguishable groups as measured using a Kruskall-Wallis test and post hoc Tukey test (p<0.05).

Figure 8

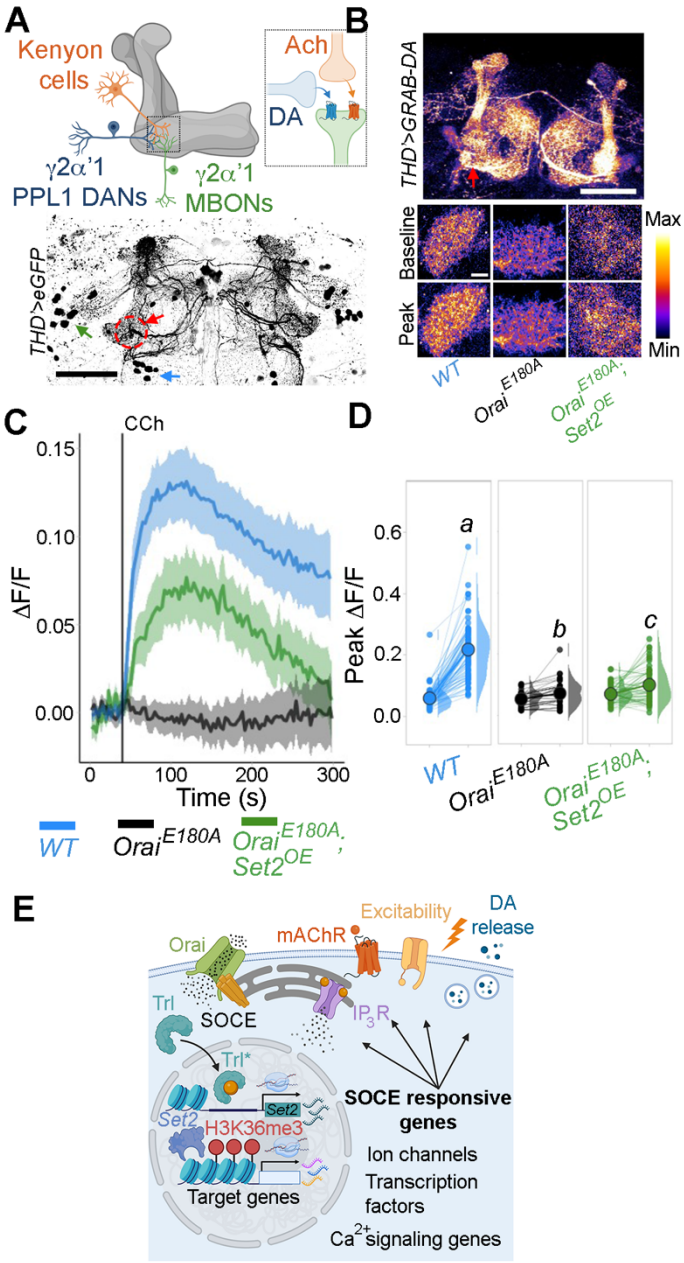

1524 **Figure 8. *THD'* DANs require SOCE-mediated gene expression for**
1525 **neuromodulatory dopamine release in the mushroom body γ lobe. A.** Schematic
1526 of a KC-DAN-MBON tripartite synapse at the γ2α'1 MB lobe (upper), innervated by
1527 fpDANs (lower). The γ2α'1 MB lobe is marked by a red circle and arrow and the fpDAN
1528 clusters are marked with a green arrow (PPL1) and blue arrow (PPM3) . Scale bar=50
1529 μM. **B**. CCh-evoked DA release measured at the γ2α'1 MB lobe using the GRAB-DA
1530 sensor expressed in *THD'* DANs. Representative GRAB-DA images of *THD'* DANs
1531 are shown with baseline and peak evoked responses in the indicated genotypes. Scale
1532 bar = 10 μM. **C**. Median GRAB-DA responses plotted as a function of time. A shaded
1533 region around the solid line represents the 95% confidence interval from 10 or more
1534 brains per genotype. **D.** Individual cellular responses depicted as a paired plot of peak
1535 responses where different letters above indicate statistically distinguishable groups
1536 after performing a Kruskal Wallis Test and a Mann-Whitney U-test. **E**. Schematic
1537 describing how Orai-mediated Ca^{2+} entry regulates expression of key genes that
1538 control neuronal activity in fpDANs.